

Neutral Beams from Blazar Jets

Armen M. Atoyan

CRM, Universite de Montreal, Montreal H3C 3J7, Canada

atoyan@crm.umontreal.ca

and

Charles D. Dermer

*E. O. Hulbert Center for Space Research, Code 7653,
Naval Research Laboratory, Washington, DC 20375-5352*

dermer@gamma.nrl.navy.mil

ABSTRACT

We treat the production of neutrons, photons, and neutrinos through photomeson interactions of relativistic protons with ambient photons in the compact inner jets of blazars. Internal synchrotron and external isotropic radiation due to scattered optical/UV accretion-disk radiation are considered as target photon fields. We characterize the conditions when the photomeson interactions of ultra-relativistic protons become effective, and show that the presence of the external radiation field makes possible strong energy losses already for protons with energies $E_p \gtrsim 10^{15}$ eV. Without this component, effective energy losses of protons begin at $E_p \gtrsim 10^{18}$ eV, and would rapidly disappear with expansion of the blob.

We develop a model describing the production and escape of neutrons from a comoving spherical blob, which continue to interact with the ambient external radiation field on the parsec-scale broad line region (BLR). Neutrons may carry $\approx 10\%$ of the overall energy of the accelerated protons with $E_p \gtrsim 10^{15}$ eV outside the BLR. Ultra-high energy gamma rays produced by photomeson interaction of neutrons outside the blob can also escape the BLR. The escaping neutrons, gamma rays, and neutrinos form a collimated neutral beam with a characteristic opening angle $\theta \sim 1/\Gamma$, where Γ is the bulk Lorentz factor of the inner jet. Energy and momentum is deposited in the extended jet from the decay of neutrons at distances $l_d(E_n) \approx (E_n/10^{17}$ eV) kpc, and through pair-production attenuation of gamma rays with energies $E_\gamma \gtrsim 10^{15}$ eV which propagate to ~ 10 -100 kpc distances. In this scenario, neutral beams of ultra-high energy gamma rays and

neutrons can be the reason for straight extended jets such as in Pictor A. Fluxes of neutrinos detectable with km-scale neutrino telescopes are predicted from flat spectrum radio quasars such as 3C 279.

Subject headings: galaxies: active — gamma-rays: theory — jets — radiation processes: nonthermal — X-rays: galaxies

1. Introduction

Multiwavelength observations of flares from blazars, particularly in the γ -ray domain, have convincingly demonstrated that the compact inner jets of blazars are effective accelerators of particles to very high energies (Hartman et al. 1999; Weekes 2000). Analyses of correlated X-ray and TeV gamma-ray flares in BL Lac objects lend support to leptonic models (Mastichiadis & Kirk 1997; Catanese et al. 1997; Pian et al. 1998; Tavecchio et al. 2001), which imply efficient acceleration of relativistic electrons in these sources, probably due to relativistic shocks. Associated acceleration of hadrons is expected with at least the same efficiency as that of the leptons, except perhaps for electron-positron pair jet models where few hadrons are present. Comparison of the radio lobe and inner jet powers indicates that jets are composed mainly of electrons and protons (Celotti & Fabian 1993), so that a nonthermal hadronic component is expected.

Acceleration of hadrons in blazar jets could be directly confirmed with the detection of neutrinos, provided that there are significant interactions of accelerated hadrons with ambient material or photon fields. Other observable consequences of hadron acceleration resulting from the same interactions that produce neutrinos can also be expected. These include X-ray and gamma-ray production from secondary leptons and gamma rays formed in hadronic interactions and, as we show here, deposition of energy transported by the escaping neutral radiations far from the inner jet.

Models invoking interactions with ambient matter (Beall & Bednarek 1999; Pohl & Schlickeiser 2000; Schuster, Pohl, & Schlickeiser 2002) require mass-loaded jets. If the nuclear interaction energy-loss time scale $t'_{pp} = (n'_p c K_{pp} \sigma_{pp})^{-1}$ is to be less than the variability time scale t'_{var} , then high plasma densities $n'_p \gg 10^9 / [t_{var}(d)(\delta/10)] \text{ cm}^{-3}$ are required, where n'_p is the comoving thermal proton density, $t_{var}(d)$ is the observed variability time scale in days, δ is the Doppler factor, $\sigma_{pp} \cong 30 \text{ mb}$ is the nuclear interaction cross section, and $K_{pp} \simeq 0.5$ is the inelasticity. (Henceforth primes denote quantities in the comoving frame.) Such models would, however, be inefficient if the sources are to be optically thin, as is required for nonthermal X-ray escape. For Thomson-thin jets ($\tau_{sc} = n'_p \sigma_T R' < 1$), the nuclear interaction

time scale

$$t'_{pp} = \frac{\sigma_T}{K_{pp} \sigma_{pp}} \frac{R'}{c\tau_T} > 40 t'_{dyn}, \quad (1)$$

where R' is the comoving blob radius, $t'_{dyn} = R'/c$ is the dynamical (or light crossing) time scale, and $\sigma_T \cong 665$ mb is the Thomson cross sections. Thus protons can only lose $\lesssim 2\text{-}3\%$ of their energy on the dynamical time scale. Moreover, as shown in Appendix A, nuclear pp interaction models require large masses and kinetic energies.

A second group of hadronic models is based upon photomeson interactions of relativistic hadrons with ambient photon fields in the jet. Most of the models of this type take into account collisions of high-energy protons with the internal synchrotron photons (Mannheim and Biermann 1992; Mannheim 1993; Mücke et al. 2002), while others also take into account external radiation that originates either directly from the accretion disk (Bednarek and Protheroe 1999) or from disk radiation that is scattered by surrounding clouds to form a quasi-isotropic radiation field (Atoyan & Dermer 2001). BL Lac objects have weak emission lines, so in these sources the dominant soft photon field is thought to be the internal synchrotron emission. Strong optical emission lines from the illumination of broad-line region (BLR) clouds in flat spectrum radio quasars (FSRQs) reveal bright accretion-disk and scattered disk radiation in the inner regions (Netzer 1990).

In the case of internal synchrotron radiation, the energy output of secondary particles formed in photohadronic processes is generally peaked in the energy range from $\approx 10^{16}\text{-}10^{18}$ eV in either low- or high-frequency peaked BL Lac objects (Mücke et al. 2002), which implies that such models can only be efficient if protons are accelerated to even higher energies. This demand upon proton acceleration for efficient photomeson production on the *internal* synchrotron photons also holds in FSRQs, which have similar nonthermal soft radiation spectra as low-frequency peaked BL Lac objects. As shown by Atoyan & Dermer (2001), however, the presence of the isotropic external radiation field in the vicinity of the jets of FSRQs strongly improves the photomeson production efficiency and relaxes the very high minimum proton energies needed for efficient production of secondaries. The existence of a strong external radiation field is required to explain (Dermer & Schlickeiser 1993, 2002; Sikora et al. 1994, 2001; Dermer, Sturner, & Schlickeiser 1997; Böttcher 2000) the luminous 100 MeV - GeV gamma-ray emission observed with the EGRET instrument on the *Compton Gamma Ray Observatory* (Hartman et al. 1996).

In the model of Atoyan & Dermer (2001), protons are assumed to be accelerated in an outflowing plasma blob moving with bulk Lorentz factor Γ along the symmetry axis of the accretion-disk/jet system. The relativistic protons are assumed to have an isotropic pitch-angle distribution in the comoving frame of a plasma blob, within which is entrained a tangled magnetic field. In our study, we determined the intensity of the internal radiation

fields based on observations of 3C 279 during the flaring state in 1996 (Wehrle et al. 1998), and calculated the high-energy neutrino flux expected under the assumption that the power to accelerate relativistic protons was equal to the power injected into nonthermal electrons which explains the observed gamma-ray emission. The presence of a quasi-isotropic external radiation field enhances the neutrino detection rate by an order-of-magnitude or more over the case where the field is absent, so we predict that FSRQs can be detected with km-scale neutrino detectors, whereas BL Lac objects are not as promising for neutrino detection. The model also takes into account the effects of relativistic neutron production, which can escape from the blob unless they are converted back to protons due to decay or further photohadronic collisions inside the blob.

In this paper, we further develop this model. Details of the theory are presented that describe the evolution of relativistic protons, taking into account photohadronic energy losses and neutron escape from the relativistically moving blob. Production of neutrons has been considered earlier in the stationary cores of AGNs (Sikora et al. 1989; Kirk & Mastichiadis 1989; Begelman et al. 1990; Giovanoni & Kazanas 1990; Atoyan 1992a,b), though not in the context of a jet model. The neutrons escaping from a relativistic blob form a beam with opening angle $\theta_n \cong \Gamma^{-1}$. These neutrons are subject to decay and further photohadronic interactions while passing through the quasi-isotropic external radiation field on the parsec scale, which we associate with the broad emission-line region (BLR). Ultra-high energy gamma rays produced from the decay of secondary pions outside the blob can escape the BLR because they are no longer subject to strong $\gamma\gamma$ interactions with the synchrotron photons inside the blob when they are at a distance of a few $\times R'$ from the blob. This results in a neutral beam of ultra-high energy (UHE) neutrons and gamma rays that can transport the energy to large distances from the central engine without significant interactions with the ambient medium until the neutrons decay or gamma rays are converted to electron-positron pairs through pair attenuation with diffuse radiation fields. This scenario naturally explains the appearance of large-scale jets that are colinear with the inner jets and appear straight on scales of hundreds of kpc. We also consider whether the different morphologies of FRI and FRII radio galaxies are a consequence of the different neutral beam properties formed in BL Lac objects and FSRQs.

In Section 2, we describe the model, our treatment of photomeson production and the energy spectra of secondaries, and our method to estimate the radiation and magnetic fields in the blob. The results of the calculations are presented in Section 3, and a discussion and summary are given in Section 4. A comparison of neutrino production through photomeson $p\gamma$ and nuclear pp interactions in jets is given in Appendix A, and the conditions when the direct accretion-disk radiation field is less important than the scattered radiation field are derived in Appendix B.

2. Model

Here we consider the production of secondaries formed through photomeson interactions between relativistic protons and photons of both the internal synchrotron and the external scattered accretion-disk radiation fields. The scattered accretion-disk field is more important than the direct accretion disk radiation field when the blob is at a distance of hundreds of Schwarzschild radii from the central engine because, unlike the case for Compton scattering, the low-energy threshold for the photomeson process requires higher energy photons in the rest frame of the proton. The effects of directionality from photons originating from the accretion disk make this component less important for photomeson production than the scattered radiation field. The energy threshold is difficult to satisfy for photons originating from the luminous central regions of the accretion disk, which enter the plasma blob in a tail-on geometry. The accretion disk photons that enter from moderate angles originate from cooler portions of the disk at large disk radii, so that higher energy protons are required to exceed the photomeson threshold energy (Bednarek and Protheroe 1999). A quantitative estimate of the relative importance of the direct and scattered radiation fields is derived in Appendix B.

For an isotropic spatial distribution of neutrons in the blob frame moving with Lorentz factor $\Gamma \gg 1$, the pattern of escaping neutrons in the stationary frame would be beamed with a characteristic opening angle $\theta \simeq 1/\Gamma$. The beaming of energetic neutrons is even more pronounced when one takes into account that the angular distribution of external radiation is highly beamed in the direction opposite to the jet in the blob frame. For isotropic protons, this will give significant preference to head-on $p\gamma$ collisions of the protons in the direction of the jet rather than in the opposite direction. Therefore, similar to the case of Compton scattering (Dermer 1995), though possibly even more pronounced due to threshold effects, the external radiation field will cause a significant directional enhancement of the high-energy neutral beams in the jet direction already in the comoving frame. We have, however, neglected this effect in the paper, and a precise treatment of this effect is deferred to later work.

In the following subsections, we present our method of calculations of photomeson and neutron production, proton energy-loss time scales and the relevant radiation fields, and spectra of secondary leptons, gamma rays, and neutrinos resulting from the decay of pions. Following this, we describe how the target photon fields are derived. We then present our treatment of proton evolution using a continuity-equation approach, and develop a theory for the neutron escape and subsequent neutron and γ -ray interactions outside the plasma blob.

2.1. Production of Secondaries in Photomeson Collisions

Photomeson interactions of relativistic protons with photons of the ambient radiation field produce secondary electrons and positrons (referred to henceforth as electrons, unless the distinction is necessary), gamma rays, and neutrinos primarily through the production and decay of pions. The relevant decay chains are $\pi^0 \rightarrow 2\gamma$, and $\pi^\pm \rightarrow \mu^\pm + \nu_\mu \rightarrow e^\pm + 2\nu_\mu + \nu_e$ (we do not distinguish between ν_μ and $\bar{\nu}_\mu$). It is important that in about half of these inelastic collisions, the primary relativistic proton will be converted to a relativistic neutron. This is true for the single-pion production channel $p + \gamma \rightarrow n + \pi^+$, which has approximately the same cross section as the channel $p + \gamma \rightarrow p + \pi^0$ without neutron production, as well as for multipion production channels.

Energy losses of relativistic protons (and neutrons) are calculated on the basis of standard expressions (e.g., Berezinskii & Grigoreva (1988)) for the cooling time of relativistic protons, $t_{p\gamma} = E_p/|dE_p/dt|$, due to photopion production in $p\gamma$ collisions. If the ambient photons have spectral density $n_{\text{ph}}(\epsilon, \Omega)$ in the direction Ω , then the cooling time of a proton in the direction Ω_p is equal to

$$t_{p\gamma}^{-1}(\gamma_p, \Omega_p) = c \int_0^\infty d\epsilon \oint d\Omega (1 - \beta_p \cos \psi) n(\epsilon, \Omega) \sigma_{p\gamma}(\epsilon_r) K_{p\gamma}(\epsilon_r), \quad (2)$$

where $\epsilon_r = \epsilon \gamma_p (1 - \beta_p \cos \psi)$ is the photon energy in the rest frame of the proton, γ_p , $\beta_p c$, and ψ are the proton's Lorentz factor, speed, and collision angle with the photon, respectively, and $K_{p\gamma}(\epsilon_r)$ is the inelasticity of the interaction. The threshold photon energy for pion production in $p\gamma$ and $n\gamma$ reactions in the rest frame of the incident nucleon is $\epsilon_{\text{th}} \approx 150$ MeV. This means that protons with, say, 1 PeV energy will effectively interact with soft X-ray photons with energy $\gtrsim 0.15$ keV.

In the case of an isotropic photon distribution where $n_{\text{ph}}(\epsilon, \Omega) = n(\epsilon)/4\pi$, equation (2) reduces to the form

$$t_{p\gamma}^{-1}(\gamma_p) = \int_{\frac{\epsilon_{\text{th}}}{2\gamma_p}}^\infty d\epsilon \frac{c n_{\text{ph}}(\epsilon)}{2\gamma_p^2 \epsilon^2} \int_{\epsilon_{\text{th}}}^{2\epsilon\gamma_p} d\epsilon_r \sigma(\epsilon_r) K_{p\gamma}(\epsilon_r) \epsilon_r \quad (3)$$

(Stecker 1968; Berezinskii et al. 1990). The $p\gamma$ collision rate $\nu_{p\gamma}(E_p)$ is given by a similar expression as equations (2) or (3), but with the inelasticity coefficient $K_{p\gamma}$ being dropped from the integral. The mean inelasticity $\bar{K}_{p\gamma}(\gamma_p) = 1/[t_{p\gamma}(\gamma_p) \nu_{p\gamma}(E_p)]$.

A detailed recent study of this photohadronic process is given by Mücke et al. (1999). To simplify calculations, we approximate $\sigma(\epsilon_r)$ as a sum of 2 step-functions $\sigma_1(\epsilon_r)$ and $\sigma_2(\epsilon_r)$ for the single-pion and multi-pion production channels, respectively, with $\sigma_1 = 380 \mu\text{b}$ for $200 \text{ MeV} \leq \epsilon_r \leq 500 \text{ MeV}$ and $\sigma_1 = 0$ outside this region, whereas $\sigma_2 = 120 \mu\text{b}$ at

$\epsilon_r \geq 500$ MeV. The inelasticity in the single pion channel is approximated as $K_{p\gamma} = K_1 \approx 0.2$, whereas $K_{p\gamma} = K_2 \approx 0.6$ for energies above 500 MeV. Our treatment of the photomeson process gives good agreement with more detailed treatments of the time scales for photo-pion interactions of ultra-relativistic cosmic rays with the cosmic microwave background (Berezinskii & Grigoreva 1988; Stanev et al. 2000). This approach also works well for a broad power-law distribution of field photons $u'_{\text{ph}}(\epsilon') \propto \epsilon'^{-\alpha}$ for different spectral indices α , and readily explains the significant increase in the mean inelasticity of incident protons (or neutrons) from $\bar{K}_{p\gamma} \simeq 0.2$ for steep photon spectra with $\alpha_\gamma \gtrsim 1$, to $\bar{K}_{p\gamma} \rightarrow 0.6$ for hard spectra with $\alpha_\gamma < 1$, giving results in good agreement with the treatment of Mücke et al. (1999).

The spectra of secondary $\pi^{0,\pm}$ -decay particles (ν, γ, e) are calculated in the δ -function approximation for the energies of the secondaries. To correctly apply the δ -function approximation, one has to properly take into account the different inelasticities of the single-pion and multi-pion production channels. In the single-pion production channel, the probability for the conversion of a proton to a neutron with the emission of a π^+ -meson is given by $\xi_{pn} \cong 0.5$. Given that the mean energies E_ν and E_e of secondary electrons and neutrinos, respectively, are approximately the same, and that the π^+ takes on average $K_1 E_p$ of the initial proton energy E_p , we have that $E_\nu \cong E_e \cong 0.05 E_p$. In the single-pion channel, a π^0 -meson is produced with the probability $1 - \xi_{pn}$, which results in two gamma-rays each with mean energy $E_\gamma \cong 0.1 E_p$ after the π^0 decay.

In the multi-pion channel, we treat the coefficient of the inelasticity $K_2 \approx 0.6$ as a result of the production of three leading high-energy pions, equally distributed between π^+ , π^- , and π^0 mesons, which becomes increasingly valid in the limit of large multiplicities. These three leading pions are assumed to take most of the energy lost by the primary proton, so that the remaining pions take away a negligible fraction of the initial energy. In this case, the mean energy carried by each pion is equal to $0.2 E_p$, and the mean energies carried by the secondary electrons, neutrinos, and gamma rays are the same as in the single-pion channels. The production spectra of the secondaries can now be found in the δ -function approximation for the differential cross sections for parent pion production, given the mean numbers of pions produced per $p\gamma$ interaction.

The mean inelasticity $\bar{K}_{p\gamma} = p_1 K_1 + (1 - p_1) K_2$ for photomeson interactions of a proton with energy E_p depends on the interaction probabilities p_1 and $p_2 = 1 - p_1$ of the proton with the given photon field via single-pion or multi-pion channels, respectively. This relation can be inverted to derive the value of $p_1 \equiv p_1(E_p)$, given by

$$p_1 = \frac{K_2 - \bar{K}_{p\gamma}(E_p)}{K_2 - K_1} . \quad (4)$$

Using the numbers of neutral and charged pions produced in single-pion and multi-pion channels, we can deduce the mean numbers of high-energy pions produced per $p\gamma$ collision at proton energy E_p . For π^0 production we thus have $n(\pi^0) = p_1(1 - \xi_{pn}) + p_2 = 1 - p_1\xi_{pn}$, and for the mean total number of charged pions $n(\pi^+ + \pi^-) = 2p_2 + p_1\xi_{pn}$. Taking further into account that 2 γ -rays are produced in π^0 decay, and that 3 neutrinos and 1 electron are produced in the decay of every charged pion, we arrive at the following formulae for the production spectra $Q_x(E) \equiv dN_x(E)/dt$ of gamma rays, electrons and neutrinos, given by

$$Q_\gamma(E_\gamma) \cong 20(1 - \xi_{pn}p_1) \nu_{p\gamma}(10E_\gamma) N_p(10E_\gamma) \quad (5)$$

$$Q_e(E_e) \cong 20(p_1\xi_{pn} + 2p_2) \nu_{p\gamma}(20E_e) N_p(20E_e) \quad (6)$$

The production spectrum of neutrinos $Q_\nu(E_\nu) = 3Q_e(E_e)$, with $E_\nu = E_e$.

2.2. Photon and Magnetic Fields

The spectral energy density of the synchrotron radiation field $u'_s(\epsilon')$, which is assumed to be isotropic in the comoving frame, depends on knowledge of the size R' of the emitting region and the νF_ν spectral fluxes $f_s(\epsilon)$ (erg cm $^{-2}$ s $^{-1}$) measured by an observer during a blazar flare. We use the variability time scale to estimate $R' \approx c\delta t_{var}/(1 + z)$ although, strictly speaking, this relation gives only an upper limit to the source size. The comoving synchrotron photon energy density is then found through the relation

$$\epsilon' u'_s(\epsilon') \cong \frac{2d_L^2 f_s(\epsilon)}{R'^2 c \delta^4} \cong \frac{2d_L^2 (1 + z)^2 f_s(\epsilon)}{c^3 t_{var}^2 \delta^6} , \quad (7)$$

where $\epsilon = \delta\epsilon'/(1 + z)$ relates photon energies in the observer and comoving frames, and d_L is the luminosity distance (see, e.g., Totani (1999)). In our calculations, we consider an $\Omega_m = 0.3$, $\Omega_\Lambda = 0.7$ cosmology with a Hubble constant of 65 km s $^{-1}$ Mpc $^{-1}$.

For the spectrum of the external UV radiation field, we use a Shakura and Sunyaev (1973) optically-thick accretion disk radiation field that is scattered by BLR clouds. The specific spectral energy density of the direct disk radiation along the jet axis in this model is given by (Dermer & Schlickeiser 2002)

$$u(\epsilon, \Omega; h) = \frac{3R_g L_{ad}}{16\pi^2 c H^3 \tan^3 \psi} \delta(\epsilon - \hat{\epsilon}) , \quad (8)$$

where L_{ad} is the total luminosity of the accretion disk, $h = H/R_g$ is the height above the accretion disk in units of gravitational radius $R_g = GM_{bh}/c^2 = 1.5 \times 10^5 M_{bh}/M_\odot$ cm for a central black hole with mass M_{bh} . This expression employs a monochromatic approximation

for the mean photon energy $\hat{\epsilon} = \epsilon_*/r^{3/4}$, where $\epsilon_* \approx 100$ eV depends weakly on M_{bh} and accretion rate (Dermer & Schlickeiser 1993, 2002), and $r = h \tan \psi$ is the accretion disk radius (in units of R_g) wherefrom originate the photons ϵ crossing the jet axis at an angle ψ . The maximum photon energy ϵ_{max} is given in this approximation by $\epsilon_*/r_i^{3/4}$, where r_i is the innermost radius of the blackbody accretion disk, and $r_i \geq 6$ for a Schwarzschild metric.

The spectrum of the isotropic component depends on the integrated disk field, which has spectral luminosity $L_{ad}(\epsilon) \propto \epsilon^{1/3} \exp(-\epsilon/\epsilon_{max})$ from the far IR up to ϵ_{max} . The quasar 3C 273 displays a pronounced UV bump peaking above ≈ 10 eV (Lichti et al. 1995). A thermal emission component is detected in a low state from the blazar 3C 279 at a temperature of ~ 20000 K, corresponding to $\epsilon_{max} \sim 5$ eV (Pian et al. 1999). This value, however, may underestimate the effective maximum temperature due to uncertainties in the modeling and subtraction of the nonthermal component. Moreover, in a flaring state, 3C 279 may have a higher accretion rate and effective accretion-disk temperature. For calculations of the spectra of a typical FR II, we take $\epsilon_{max} = 20$ eV. For $\epsilon_* \approx 100$ eV this implies an effective disk innermost radius $r_i \simeq 8$.

The energy density of the quasi-isotropic component of the surrounding radiation field can be approximated by the expression

$$u_{ext}(\epsilon) \cong \frac{L_{ad}(\epsilon)\tau_T}{2\pi R_{BLR}^2 c}, \quad (9)$$

where R_{BLR} is the effective radius of the BLR, and τ_T is the Thomson depth of the BLR.¹ The energy density of the external radiation field in the jet frame is $u'_{ext} \cong \Gamma^2 u_{ext}$, where $u_{ext} = \int_0^\infty d\epsilon u_{ext}(\epsilon)$.

The quantities L_{ad} , τ_T , and R_{BLR} which define the energy density of isotropic external field component in equation (9) are not well-known for specific sources. The quantity u'_{ext} can also be estimated from the ratio of the νF_ν peak flux f_{EC}^{pk} of the γ -ray Compton component to the peak flux f_s^{pk} observed in the lower frequency nonthermal synchrotron component. Assuming that the observed 100 MeV - GeV fluxes as observed with EGRET from FSRQs in the flaring state are primarily due to Compton-scattered radiation from external photon fields, then

$$u'_{ext} \cong g u'_B \frac{f_{EC}^{pk}}{f_s^{pk}}, \quad (10)$$

¹Note that the factor 2π in the denominator of equation (9), instead of the commonly used 4π , corresponds to the fact that we are considering the photon density not outside, but inside the emission region (Atoyan & Aharonian 1996).

where $u'_B = B'^2/8\pi$ is the comoving magnetic-field energy density, and $g \gtrsim 1$ is a parameter that corrects for the Klein-Nishina effect in the observed 100 MeV - GeV fluxes.² For definiteness, note that the Klein-Nishina transition occurs when the parameter $b = 4\gamma\epsilon'_0/(m_e c^2)$ exceeds unity (Blumenthal and Gould 1970). This implies that 20 eV UV target photons will be scattered in the Klein-Nishina regime in order to produce gamma rays with energies exceeding $\approx 800/(1+z)$ MeV (independent of Γ). As shown by our numerical calculations, this requires that $g \sim 3$ for the parameters of 3C 279 that we consider.

The magnetic field B' in the blob can be determined by introducing the equipartition parameter $\eta = u'_e(1+k_{pe})/u'_B$ for the ratio of relativistic electron to magnetic-field energy densities in the jet, with the factor $k_{pe} = u'_p/u'_e$ correcting for the contribution of nonthermal hadrons to the particle energy density. We assume $k_{pe} = 1$ in the estimate of B' . The energy density in nonthermal electrons is inferred from the measured synchrotron flux density $F_s(\nu) \propto \nu^{-\alpha}$ in the range $\nu_0 \leq \nu \leq \nu_1$, with $\alpha \cong 0.5$. This gives the magnetic field

$$B'(\text{Gauss}) \cong 130 \frac{d_{28}^{4/7} f_{-10}^{2/7} [(1+k_{pe}) \ln(\nu_0/\nu_1)]^{2/7} (1+z)^{5/7}}{\eta^{2/7} [t_{\text{var}}(\text{d})]^{6/7} \delta^{13/7} \nu_{13}^{1/7}}, \quad (11)$$

and the equipartition magnetic field corresponds to the parameter $\eta = 1$. Here $\nu_{13} \equiv \nu/10^{13}$ Hz is the frequency where the flux $f_s(\epsilon) \equiv 10^{-10} f_{-10}$ ergs cm⁻² s⁻¹ is measured.

An alternative estimate of B' can be derived from the ratio of the synchrotron self-Compton (SSC) γ -ray and synchrotron peak fluxes $f_{SSC}^{pk}/f_s^{pk} \cong u'_s/u'_B$ (Sikora 1997; Tavecchio et al. 1998). Thus $u'_B = A u'_s = A f_s^{pk} (2d_L^2/R'^2 c \delta^4)$, where $A \equiv (f_s^{pk}/f_{SSC}^{pk})$. This gives

$$B'(\text{Gauss}) = \frac{4\sqrt{\pi}(1+z)d_L}{c^{3/2}\delta^3 t_{\text{var}}} \sqrt{A f_s^{pk}} \cong 1.6 \frac{d_{28}(1+z)\sqrt{Af_{-10}}}{(\delta/10)^3 t_{\text{var}}(\text{d})}. \quad (12)$$

This equation assumes that Klein-Nishina effects for the SSC γ rays are unimportant, because the Compton process occurs on softer (radio-optical) photons as compared to the UV photons for external Compton scattering. In both equations (11) and (12), the strongest dependence of B' is through the unknown Doppler factor. By equating these two equations, we can derive an estimate for δ , given by

$$\delta \cong 8.9 \frac{d_{28}^{3/8} (1+z)^{1/4} f_{-10}^{3/16} A^{7/16} \eta^{1/4} \nu_{13}^{1/8}}{[(1+k_{pe}) \ln(\nu_1/\nu_0)]^{1/4} [t_{\text{var}}(\text{d})]^{1/8}}. \quad (13)$$

²This estimate does not take into account the different beaming factors for the two processes (Dermer, Sturner, & Schlickeiser 1997), but is valid when $\Gamma \cong \delta$.

2.3. Energy Distribution of Protons and of Escaping Neutrons

Relativistic neutrons, being essentially unaffected by magnetic fields, can escape from a blob if their Lorentz factor γ_n is sufficiently large so that they do not decay into protons on the decay timescale $\tau_d(\gamma_n) = \tau_0 \gamma_n$, where $\tau_0 \simeq 910$ s is the decay time of a neutron at rest. Moreover, the neutrons must not be converted back to protons in further photomeson interactions with ambient photons inside the blob during the crossing time $t_{\text{cross}} \simeq R'/c$ needed, on average, for a neutron to leave the blob. This leakage must be taken into account in the kinetic equation describing the evolution of the proton energy distribution $N_p(E, t)$ in the blob at time t (allowing for the possibility of a non-stationary source). We develop a formalism for the evolution of the proton distribution that properly treats the possible escape of protons while in the neutron state.

The distribution $N_p(E, t)$ can be calculated in the framework of the approximation of continuous energy losses. Even though inelasticities up to $K_{p\gamma} \cong 0.5$ can be reached in photomeson interactions, the continuous energy-loss approximation is reasonable as follows from the analytic solution for the kinetic equation of relativistic particles when both continuous and catastrophic energy losses are taken into account (Atoyan 1992b). The kinetic equation for $N_p(E, t)$ is then given by

$$\frac{\partial N_p}{\partial t} = \frac{\partial}{\partial E} (P_{p\gamma} N_p) - \frac{N_p}{\tau_{\text{esc}}} + Q_p, \quad (14)$$

where $Q_p \equiv Q_p(E, t)$ is the particle injection rate, and $P_{p\gamma}(E) = -(dE/dt)_{p\gamma}$ is the proton energy loss rate due to $p\gamma$ interactions. Note that $P_{p\gamma}$ includes *both* the channels with and without conversion of the incident proton to the neutron, namely $p + \gamma \rightarrow p + \pi^0 + X$ and $p + \gamma \rightarrow n + \pi^+ + X$. This can be done because in photomeson interactions the energy loss rate of a *neutron* that is produced in the latter interaction chain is practically the same as of the proton in the first chain. Therefore once the nucleon returns to the proton pool inside the blob, it does not ‘remember’ that during some time $\Delta t < t_{\text{cross}}$ it was in the ‘neutron’ state. In other words, the energy loss of protons remaining in the blob would depend only on the overall time they spend in the blob after their injection.

The parameter $\tau_{\text{esc}} \equiv \tau_{\text{esc}}(E)$ corresponds to the characteristic escape time of protons from the blob. This should generally take into account the escape of protons both due to direct escape from the blob while in the neutron state, as well as due to diffusive escape. In this section, we neglect diffuse escape effects, although this process is taken into account to determine the spectra of protons at the highest energies in the numerical calculations. The solution to equation (14) is

$$N_p(E, t) = \frac{1}{P_{p\gamma}(E)} \int_{-\infty}^t P(\varepsilon_{t_1}) Q(\varepsilon_{t_1}, t_1) \exp \left(- \int_{t_1}^t \frac{dx}{\tau_{\text{esc}}(\varepsilon_x)} \right) dt_1. \quad (15)$$

The parameter $\varepsilon_{t_1} \equiv \varepsilon(E, t, t_1)$ corresponds to the initial energy of a particle at an earlier time t_1 which cools down to a given energy E by the time t ; thus $\varepsilon(E, t, t_1 = t) = E$. It is determined from the equation

$$t - t_1 = \int_E^{\varepsilon_{t_1}} \frac{dE}{P_{p\gamma}(E)}. \quad (16)$$

Note that the running time t_1 can be formally both smaller and larger than the time t at which the particle energy E is given, i.e., ε is simply a trajectory of such particle in the energy space.

The characteristic escape time of protons can be evaluated if we recall that $\Delta N_{\text{esc}} = (N_p/\tau_{\text{esc}}) \times \Delta t$ is the number of particles escaping the source during the time interval Δt . It can be written also as $\Delta N_{\text{esc}}/\Delta t = \xi_{\text{esc}} \dot{N}_p = \xi_{\text{esc}} \xi_{pn} \nu_{p\gamma}(E) N_p(E, t)$, where $\xi_{pn} \equiv \xi$ ($\cong 0.5$) is the probability of conversion of a proton into the neutron per one $p\gamma$ collision, $\nu_{p\gamma}$ is the frequency of such collisions, and ξ_{esc} is the probability that the produced neutron would escape the blob prior to its conversion back to the proton state. Thus

$$\frac{1}{\tau_{\text{esc}}(E)} = \xi_{\text{esc}}(E) \xi_{pn} \nu_{p\gamma}(E). \quad (17)$$

In order to calculate ξ_{esc} , consider the solution to the equation

$$\frac{\partial N_n}{\partial t} = \frac{\partial}{\partial E} (\xi_{nn} P_{n\gamma} N_n) - (\xi_{np} \nu_{n\gamma} + 1/\tau_d) N_n + Q_n \quad (18)$$

for the energy distribution of neutrons $N_n(E, t)$ in the blob, assuming instantaneous injection at time $t_0 = 0$, which corresponds to the source function $Q_n(E, t) = N_0(E) \delta(t - t_0)$. In this equation, $P_{n\gamma}$ and $\nu_{n\gamma}$ represent the overall photomeson energy loss and collision rates of the neutrons, respectively, which are approximately the same as the respective rates for the proton photomeson interactions. Unlike in eq. (14) for the protons, however, we now have to take into account that after each photomeson collision, a neutron either remains neutron with probability ξ_{nn} ($\cong 0.5$) while losing energy, or is converted to a proton and returns to the proton pool with probability $\xi_{np} = 1 - \xi_{nn}$. The neutron escape term also takes into account the decay of neutrons $n \rightarrow p + e^+ + \nu$ on timescale $\tau_d = \tau_d(E)$, with $E_n \cong E_p$.

The solution to equation (18) is given in general by equation (15). For the instantaneous injection function $Q_n(E, t) = N_0(E) \delta(t)$, equation (15) reduces to

$$N_n(E_1, t_1) = \frac{P_{n\gamma}(E) N_0(E)}{P_{p\gamma}(E_1)} \exp \left[- \int_0^{t_1} \left(\frac{1}{\tau_d(E_x)} + \xi_{np} \nu_{n\gamma} \right) dx \right]. \quad (19)$$

Here we use E_1 for the running energy at t_1 , while reserving E for the initial neutron energy. Note that in the continuous energy loss-approximation, E should be the same as the energy of the parent proton.

Because the neutrons escaping the source are the ones which survive during the time $t_1 \geq t_{\text{cross}} \simeq R'/c$ after injection, the escape probability ξ_{esc} is formally the ratio $N_n(E_1, t_1)\Delta E_1/N_0(E)\Delta E$ at time $t_1 = t_{\text{cross}}$. Taking also into account that, using equation (16), the ratio of the energy intervals $\Delta E_1/\Delta E = P(E_1)/P(E)$, we find that

$$\xi_{\text{esc}} = \exp \left[- \int_0^{t_{\text{cros}}} \left(\frac{1}{\tau_d(E_x)} + \xi_{np}\nu_{n\gamma}(x) \right) dx \right]. \quad (20)$$

This defines the effective time of proton escape $\tau_{\text{esc}}(E)$ via equation (17). The evolution of neutrons outside the blob is given by equation (18) with the source function $Q_n \equiv Q_n(E, t)$ equal to the rate of escaping protons from the blob in equation (14), i.e., $Q_n = N_p/\tau_{\text{esc}}$.

3. Results of Calculations

We calculate the spectra of protons, neutrons, and secondaries from photomeson interactions, taking inner jet parameters derived from quasi-simultaneous observations (Wehrle et al. 1998) of the 1996 flare from 3C 279 as typical for FSRQs. For calculations of the photomeson production effects in low luminosity blazars, we use parameters of the blob derived from flaring states of the BL Lac object Mrk 501 (Catanese et al. 1997; Pian et al. 1998).

3.1. Photopion Production in FSRQs

The redshift of 3C 279 is $z = 0.538$, which implies a luminosity distance $d_L \cong 1.05 \times 10^{28} \text{ cm}$ for an $\Omega_m = 0.3$, $\Omega_\Lambda = 0.7$ cosmology with a Hubble constant of $65 \text{ km s}^{-1} \text{ Mpc}^{-1}$. We use parameters derived for the flaring state of 3C 279 during 1996 February 4-6 (Wehrle et al. 1998). Note that parameters appropriate to the extended 3 week quiescent state of the same observing period were used earlier in Atoyan & Dermer (2001). The measured variability time scale $t_{\text{var}} \cong 1 \text{ day}$ for the 1996 flare of 3C 279 implies a characteristic source size

$$R' \cong ct_{\text{var}}\delta/(1+z) \cong 1.7 \times 10^{16} t_{\text{var}}(d)(\delta/10) \text{ cm}. \quad (21)$$

For calculations of $n'_s(\epsilon') = u'_s(\epsilon')/\epsilon'$ in equation (7), we approximate the flux density $F_s(\epsilon) = f_s(\epsilon)/\epsilon \propto \epsilon^{-\alpha}$ observed during the flare of 1996 (Wehrle et al. 1998) in the form of a continuous broken power-law function, with indices $\alpha_1 \cong 0.5$ at frequencies $\nu_0 \cong 10^{11} \text{ Hz} < \nu = \epsilon/h \leq \nu_1 = 10^{13} \text{ Hz}$, $\alpha_2 \cong 1.45$ at $\nu_1 \leq \nu \leq \nu_2 = 10^{16} \text{ Hz}$, and $\alpha_3 \cong 0.6$ at $\nu \geq \nu_2$. The νF_ν synchrotron radiation flux reaches its maximum value $f_s^{pk} = f_s(\epsilon_{pk}) \cong 1.7 \times 10^{-10} \text{ erg cm}^{-2} \text{ s}^{-1}$ at $\epsilon = \epsilon_{pk} = h\nu_1$. The flaring flux of the Compton γ -ray component peaks at $\sim 500 \text{ MeV}$, and is ~ 15 larger than f_s^{pk} during the flare (Wehrle et al. 1998).

Spectral models for 3C 279 show that a complete spectral fit requires that the ratio of synchrotron to SSC peak fluxes $A \simeq 1$ (Böttcher 1999; Hartman et al. 2001). This implies from equation (13) that $\delta \simeq 6$, which is just above the lower limit $\delta \geq 5$ required from the condition that the gamma rays in the jet be transparent to $\gamma\gamma$ pair attenuation (Atoyan & Dermer 2001). In the calculations, we treat a range of Doppler factors $\delta = 6, 10$ and 15 , noting that there can be uncertainties in our knowledge of A , as well as departures from equipartition. Note, however, that the range of the Doppler factors cannot be very large due to the weak dependence of δ on the uncertain parameters. The magnetic field is then derived from equation (11).

During the 1996 February 4-6 flare, a mean apparent isotropic ‘ 4π ’ γ -ray luminosity of 10^{49} ergs s^{-1} was measured with EGRET. Assuming that the power injected in relativistic protons is equal to the power observed in γ rays, we take for the comoving proton luminosity $L'_p = 10^{49}/\delta^4$ ergs s^{-1} . The injection of protons takes place during the time $t_{inj} = 2$ days in the observer frame, corresponding to the time $\delta t_{inj}/(1+z)$ in the comoving blob frame. For the spectrum of protons, we take $Q_p(E_p) \propto E_p^{-2} \exp(-E_p/E_{max})$, where E_{max} is defined by the condition that the proton gyroradius does not exceed R' and that the proton cooling rate $t_{p\gamma}^{-1}(E_p)$ does not exceed the maximum acceleration rate given by eBc/E_p . The BLR radius R_{BLR} is deduced from equation (9) with the assumption $\tau_T = 0.1$. Equation (10) is used to estimate the external radiation density $u'_{ext}(\epsilon')$ in the blob frame, noting that $\epsilon' u'_{ext}(\epsilon') \cong \Gamma^2 \epsilon u_{ext}(\epsilon)$ (e.g., Dermer & Schlickeiser 2002). This approach results in a dependence of the BLR radius on δ (which we assume to be equal to Γ), $R_{BLR} = 0.11$ pc and 0.47 pc for $\delta = 6$ and $\delta = 10$, respectively. For the range of Doppler factors used in our calculations, the blob remains within the BLR during the entire time of injection of relativistic protons.

Fig. 1 shows the spectra of protons and escaping neutrons and gamma rays for $\delta = 6$ and $\delta = 10$ in Figs. 1a and 1b, respectively. The dotted curves show the overall spectra of protons injected into the blob, and the thin solid curves show the spectra of protons which remain in the blob by the time that the blob reaches the edge of the BLR at stationary-frame time $t = R_{BLR}/c$. The thick solid curves show the overall spectra of neutrons which escape from the relativistic blob during the time of its propagation through the BLR. The feature in the neutron spectrum between 10^{15} and 10^{16} eV in Fig. 1a and, to a lesser extent, in Fig. 1b, is due to the neutron energy losses on the external radiation field which are only significant above $\sim 10^{15}$ eV. The magnetic fields for the $\delta = 6$ and $\delta = 10$ cases in Figs. 1a and 1b are equal to 18.1 G and 7 G, respectively. The corresponding characteristic maximum energies of the accelerated protons in these two cases are equal to 2.5×10^{18} eV and 6.5×10^{18} eV in the blob frame, which are translated to energies by a factor of $\Gamma \simeq \delta$ times higher in the stationary frame.

Neutrons escaping from the blob moving with Lorentz factor Γ will form a highly collimated beam with opening angle $\theta \sim 1/\Gamma$. These neutrons continue to interact with the external radiation field through photopion production, and are also lost through decay. Both effects modify the neutron spectra until the neutrons reach the edge of the BLR. The spectra of surviving neutrons which reach the edge of the external UV BLR field are shown by the dashed curves. Photomeson interactions of neutrons outside the blob result in the production of a beam of ultra-high energy neutrinos, electrons, and gamma rays with opening angle $\sim 1/\Gamma$. The expected number of neutrinos to be detected with ground-based neutrino telescopes is calculated below. The electrons may be deflected by the magnetic field in the BLR to produce synchrotron or Compton-scattered radiation, but we do not consider this emission further here because the fluxes will depend significantly on unknown properties of the medium outside the jet, such as the magnetic field strength and geometry.

The spectra of π^0 -decay gamma rays produced by neutrons outside the blob which escape from the BLR without undergoing subsequent $\gamma\gamma$ interactions are shown by the dot-dashed curves in Fig. 1. These gamma rays have very high energies, ranging from 10^{14} to 10^{18} eV. The thin curves in Fig. 2 show the $\gamma\gamma$ pair-production opacity due to interactions of gamma rays with photons of the BLR, calculated for a gamma ray traversing the radius of the BLR. Also shown by the heavy curves are the $\gamma\gamma$ opacities within the blob. This figure demonstrates that gamma rays produced within the blob are subject to very strong attenuation, and therefore have no chance to escape. The attenuation is also very strong for photons produced outside the blob in the BLR unless these photons have very high energies ($\gtrsim 10^{16}$ eV) or are produced close to the edge of the BLR. The peak feature in the escaping γ -ray spectrum between 10^{14} and 10^{15} eV in Fig. 1a is due to the threshold character of photomeson interactions of neutrons with the external radiation field, which continue to produce gamma rays until they reach the edge of the BLR.

We calculate the fraction of energy initially injected in the form of protons above 10^{15} eV, $W_p(> 10^{15}\text{eV})$, which is taken away from the blob in the form of neutrons. For the cases of $\delta = 6$ and 10, as shown in Fig. 1, these fractions are 14.2% and 25.6%, respectively. Neutrons with energies greater than 10^{17} eV that escape from the the BLR will decay on length scales

$$l_d \approx 1 (E_n/10^{17}) \text{ kpc} \quad (22)$$

The fraction of injected relativistic proton energy $W_p(> 10^{15}\text{eV})$ carried by these neutrons, which we denote by $W_n(> 10^{17}\text{eV})$, is equal to 0.00012 % and 2.3% for $\delta = 6$ and 10, respectively, for the parameters used in Fig. 1. The fraction of ultrarelativistic energy that escapes from the BLR in the form of gamma rays above 10^{15} eV is equal to 0.19% and 5.1% for $\delta = 6$ and 10, respectively. The fact that a smaller fraction of initial energy is taken away by neutrons for $\delta = 6$ than for $\delta = 10$ is explained by the stronger external radiation

field in the former case. This is a consequence of the strong dependence of the inferred external radiation field energy density $u'_{ext} \propto \delta^{-26/7}$, as follows from equations (10) and (11), which strongly attenuates the beam of neutrons escaping the blob close to the black hole. Our calculations show that the fraction of injected energy in ultrarelativistic protons, $W_p(> 10^{15} \text{ eV})$, that escape the BLR in the form of neutrons and gamma rays can reach $\sim 10\%$ for different model parameters, when attenuation of the neutrons escaping the BLR is not very strong. In particular, the yield in neutrons leaving the BLR is always high if the proton acceleration in the blob occurs not during a short flaring period, as in Fig. 1, but during the time $t \sim t_{BLR} = R_{BLR}/c$ when the blob is traveling through the isotropic external radiation field. On the other hand, a higher rate of degradation of neutrons results in higher fluxes of neutrinos produced both inside and outside the blob. Fig. 3 shows the fluences of neutrinos integrated over several days in the observer frame determined by the time for the blob to pass through the BLR, for the same parameters as used in Fig. 1. The solid and dashed curves show the fluences calculated for $\delta = 6$ and 10 , respectively. The thick and thin curves represent the fluences of neutrinos produced by photopion interactions inside and outside the blob, respectively. For the spectral fluences shown in Fig. 3, the total number N_ν of neutrinos that could be detected by a 1 km^3 detector such as IceCube, calculated using neutrino detection efficiencies given by Gaisser, Halzen, & Stanev (1995), are 0.29 and 0.078 , for $\delta = 6$, and 0.13 and 0.076 , for $\delta = 10$, where the pair of numbers refer to neutrinos formed inside and outside the blob, respectively.

The dot-dashed and the triple-dot-dashed curves represent the neutrino fluences that would be expected for the same time scales and source parameters, but neglecting interactions with the external radiation field. The numbers of neutrinos that are predicted to be detected by a 1 km^3 detector in this case are more than an order-of-magnitude lower, and are 0.030 and 0.0047 for $\delta = 6$ and 10 , respectively. As previously noted (Atoyan & Dermer 2001), the presence of external radiation fields is crucial for prospects to detect neutrinos from blazars with high-energy neutrino telescopes.

In order to understand how the production of neutrons will change when the inner jet expands, we show in Figs. 4a and 4b the spectra of protons and escaping neutrons and gamma rays, as in Fig. 1, but calculated for different sizes of the blob corresponding to $t_{var} = 0.3$ and 3 days, with $\delta = 10$. Here we have fixed the external radiation field density and size of the BLR ($R_{BLR} = 0.41 \text{ pc}$) to the values derived in Fig. 1b for $\delta = 10$. Moreover, we assume that the acceleration rate of protons is such that the same amount of total energy as in Fig. 1 is injected in the protons continuously during the entire period that the jet travels through the BLR. The fractional energy taken away by neutrons from the compact blob and from the BLR is $\approx 30\%$ and $\approx 7.5\%$, respectively, for $t_{var} = 0.3 \text{ d}$. In the case of the inflated blob with $t_{var} = 3 \text{ d}$, these fractions drop down correspondingly to 12% and 2.4% .

In Fig. 5 we show the radiation fluxes produced in, and escaping from the blob following the electromagnetic cascade initiated by energetic pion-decay electrons and gamma rays for the case $\delta = 10$. Fig. 5a shows the cascade radiation spectra at the maximum, which is reached at time $t = 2$ d when the injection of new accelerated protons in the blob stops. Fig. 5b shows the radiation fluxes at the time when the blob is leaving the external radiation field region. The thick and thin curves correspond to synchrotron and Compton-scattered radiation, respectively. The radiation of the first generation of electrons, which includes both the electrons from π^\pm decays and the electrons produced by absorption of π^0 -decay gamma rays in the blob, are shown by the solid curves. The synchrotron radiation strongly dominates the Compton-scattered emission in the first generation because the electrons of the first generation are ultra-relativistic, such that Compton scattering is in the extreme Klein-Nishina regime. The second, third, and fourth generations of the cascade radiation are shown by the dashed, dot-dashed, and triple-dot dashed curves, respectively. The heavy dots show the total spectrum. As can be seen, emission above 1 GeV can escape from the blob and BLR. These figures show that in both cases the main contribution to the resulting gamma-ray flux is due to synchrotron radiation of the first generation of the cascade electrons born mostly with energies above 10^{14} eV.

Noticeable gamma-ray fluxes may also be produced by secondaries from $p\gamma$ interactions in the blob at later stages when the blob is still within the BLR, as seen in Fig. 5b. One may also expect that ~ 10 GeV gamma-ray photons produced at these later stages can be due to the escaping neutrons interacting with the UV photons outside of the BLR.

3.2. Photopion Production in BL Lac Objects

BL Lac objects have generally lower luminosity than FSRQs and have weak or absent line emission, suggesting that the column density of the gas in the central parsec region is smaller. This may be due to a reduction in the fueling rate as the surrounding gas accretes onto the central engine (Böttcher & Dermer 2002; Cavalieri & D’Elia 2002). If this scenario is correct, then the mean black hole masses in BL Lac objects should be even greater than in FSRQs. Consequently, the maximum temperature of the disk in a BL Lac object should be significantly lower than in FSRQs (recall that $\epsilon_{max} \propto M_{bh}^{-1/4}(\dot{M}c^2/L_{Edd})^{1/4}$, where L_{Edd} is the Eddington luminosity and \dot{M} is the mass accretion rate; see Dermer & Schlickeiser 2002). In our calculations, we take $\epsilon_{max} = 3$ eV for BL Lac objects.

We consider Mrk 501, a high-frequency peaked BL Lac object that has been observed at TeV energies, as representative of this class of sources. Mrk 501 has a dshift $z = 0.034$, so that $d_L = 160$ Mpc. Variability has been detected on time scales as short as 1 hour,

although variability on time scales of order 1 day are also common. We therefore consider both $t_{var} = 0.1$ and 1 day (Quinn et al. 1999; Sambruna et al. 2000). For the compact jet with $t_{var} = 0.1$ d, we approximate the flux density using the April 16th, 1997 flare data (Pian et al. 1998), with indices $\alpha_1 \cong 0.5$ at frequencies $\nu_0 \cong 10^{11}$ Hz $< \nu = \epsilon/h \leq \nu_1 = 10^{18}$ Hz, and $\alpha_2 \cong 1$ at $\nu_1 \leq \nu \leq \nu_2 = 10^{20}$ Hz, and assuming a very steep cutoff above ν_2 . The νF_ν flux has reached the level of $\sim 6 \times 10^{-10}$ ergs cm $^{-2}$ s $^{-1}$. For the ‘quiescent’ state with $t_{var} = 1$ day, which may correspond to a less powerful but continuous jet, we approximate the spectral fluxes with the same power-law indices α , but with break frequencies $\nu_1 = 3 \times 10^{14}$ Hz and $\nu_2 = 3 \times 10^{17}$ Hz, and a maximum νF_ν flux at the level of 3×10^{-11} ergs cm $^{-2}$ s $^{-1}$.

Fig. 6 shows the total energy spectrum of injected protons and protons remaining in the blob at the time when the jet is at a distance $R = 0.3$ pc, which we assume to be the effective radius of the region where there is an isotropic scattered radiation field. In this calculation, we treat the $t_{var} = 1$ d case, and let $\delta = 10$. This results in an equipartition magnetic field $B_{eq} \cong 0.37$ G, and a maximum energy of accelerated protons equal to 9×10^{17} eV in the comoving frame, which is larger by a factor $\Gamma \sim 10$ in the stationary frame. For the external field, we assume that the maximum flux of the disk radiation cannot exceed the flux of 3×10^{-11} ergs cm $^{-2}$ s $^{-1}$ observed in the optical/UV range. The intensity of the isotropic radiation field is calculated assuming $\tau_T = 0.01$. For these parameters of external radiation-field, there is essentially no photomeson production by neutrons outside the blob, and consequently very low gamma-ray production outside the blob (dot-dashed curve).

The production of high-energy neutrons inside the blob through photomeson interactions with the internal synchrotron photons is still very effective for the highest energy protons with $E_p \gtrsim 10^{17}$ eV. The fraction $W_n(> 10^{17}\text{eV})/W_p(> 10^{15}\text{eV}) = 0.12$, and practically all of this neutron energy is carried from the supposed isotropic external radioation to kpc scales. The maximum energy of protons is, however, smaller compared with the $\delta = 10$ case for 3C 279 (Fig. 1), which implies a shorter propagation distance for the ultra-high energy (UHE) neutron beam. The power deposited in the neutron beam during the flare is $\gtrsim 4$ orders of magnitude smaller than the power of neutrons escaping the BLR in Fig. 1. Moreover, for larger Doppler factors, $\delta \sim 15\text{--}45$, which are implied by the modeling of TeV and X-ray flares (Pian et al. 1998; Krawczynski, Coppi, & Aharonian 2002), the power in neutrons would decrease further. Our calculations show that $W_n(> 10^{17}\text{eV}) \approx 2.6 \times 10^{46}$ and 3.6×10^{44} ergs for $\delta = 10$ and 25, respectively. Note that the fraction of energy carried by $E_\gamma > 10^{15}$ eV gamma-rays produced by neutrons escaping the blob in the isotropic external radiation region in Fig. 1 is absolutely negligible, $W_\gamma(> 10^{15}\text{eV})/W_p(> 10^{15}\text{eV}) \approx 4.7 \times 10^{-5}$

In Fig. 7, we show the fluxes calculated for the case $t_{var} = 0.1$ d, assuming $\delta = 25$. Fig. 7a is calculated for $B' = B_{eq} = 0.5$ G, corresponding to equipartition as defined in equation

(11), whereas Fig. 7b assumes $B' = 0.2 B_{eq} = 0.1$ G. The latter case may be of interest because the spectral fits for the 16 April 1997 flare in Mrk 501 seem to require fields well below equipartition. The maximum energies of accelerated protons in the stationary frame are then $E_{max} \cong 7.5 \times 10^{18}$ eV and $E_{max} = 1.5 \times 10^{18}$ GeV in Figs. 7a and 7b, respectively, so that the effective maximum energy of the neutrons escaping the inner jet (and therefore also the weak external radiation field) does not significantly exceed 10^{18} eV, as seen in Fig. 7. This suggests that in BL Lac objects, the transport of energy by ultra relativistic neutrons is still possible, but the maximum distances for energy transport by the neutrons will be significantly shorter than in FSRQs. Note also that the number of neutrinos to be expected by a km-scale neutrino detector in these two cases is extremely low, being less than 10^{-6} in both Figs. 7a and 7b.

4. Discussion and Summary

Observations of powerful gamma-ray flares from blazars with EGRET and ground-based gamma-ray telescopes have confirmed that radio-loud AGNs accelerate particles to GeV and TeV energies, respectively. Particle acceleration to higher energies may occur, but this cannot be established through gamma-ray observations because of attenuation by ambient and diffuse extragalactic optical and infrared radiation fields. Although leptonic models have been successful in fitting the spectra of blazars, models of first-order Fermi acceleration at both nonrelativistic and relativistic shocks imply that acceleration proceeds more effectively for protons than for electrons, because the Larmor radius of a particle involved into the acceleration process must be larger than the shock width, which is more easily satisfied by hadrons (e.g., Gallant 2002). The large proton-to-electron ratio in the galactic cosmic rays supports this contention. Thus our underlying assumption that protons are injected with at least the same power as inferred from the measured gamma-ray luminosity of a blazar seems reasonable.

Evidence for the acceleration of relativistic protons and heavier nuclei in blazar jets can be provided by three lines of evidence as described in the following subsections. First, hadronic acceleration could be established indirectly by detection of spectral features in the electromagnetic radiation produced by secondaries of the inelastic interactions of high-energy hadrons in blazar jets. The second and most compelling line of evidence will be provided through the direct detection of high-energy neutrinos by km-scale detectors such as IceCube.³ The third line of evidence involves consequences of the production of UHE

³<http://icecube.wisc.edu/>

neutrons and gamma-rays which transport significant amounts of energy from the central region of an AGN to large distances (Atoyan & Dermer 2001). This last feature is sufficiently interesting that we devote a separate subsection to applying this model to explain observed features of radio-loud AGNs. Finally we summarize, considering also the possibility that ultra-high energy cosmic rays (UHECRs) are accelerated in the inner jets of blazars.

4.1. Electromagnetic Radiation from Nonthermal Hadrons

Discriminating between hadronic and leptonic origins of the gamma radiation from blazars or other classes of sources is possible, although not an easy or a straightforward task. If the emission has a hadronic origin, then the emerging gamma-ray spectrum results from a cascade induced by high-energy secondary leptons and gamma-rays. Photon spectral indices from cascade radiation tend to be rather hard, and take values between 1.5 and 2.0 in the medium-energy gamma-ray regime explored by EGRET and *GLAST*⁴ (see Fig. 5). But this is also a common feature for gamma-ray spectra from an electron-photon cascade independently of whether the cascade is initiated by electrons and gamma-rays of secondary (pion-decay) origin or by primary (directly-accelerated) electrons.

A principal difference between the hadronic and leptonic induced cascades does, however, exist. It consists in a very significant contribution of the synchrotron radiation of the ultra-relativistic electrons (including the ones from the absorption of π^0 -decay gamma-rays) of the first cascade generation in the high energy gamma-ray flux in the case of hadronic initiation of the cascade. The Lorentz factor of these electrons $\gamma \gg 10^8$ is much higher than the maximum possible Lorentz factor for primary electrons, which is limited by synchrotron losses in the strong magnetic fields $B \gtrsim 0.1\text{-}10\text{ G}$ characteristic for the inner jets of blazars. As a result, the synchrotron radiation of these electrons can greatly exceed the characteristic maximum energy $E'_{s,\text{max}} \sim 25\text{ MeV}$ (e.g., de Jager et al. 1996) for synchrotron emission of directly accelerated electrons, as is apparent from Fig. 5. Additionally taking into account the Doppler boosting of the energy $E_{s,\text{max}}$ when transforming to the observer's frame, we can say that confirmation of a significant contribution of hard-spectrum synchrotron flux in the gamma-ray flares at $\gtrsim 0.1\text{ GeV}$ with *GLAST* could become a strong argument in favor of UHE hadron acceleration in the jets.

A synchrotron contribution could be confirmed experimentally by the detection of a significant polarization in the total flux, but neither *GLAST* nor other high energy gamma-ray detectors yet have the capability for the relevant measurements. It is possible that

⁴<http://glast.gsfc.nasa.gov>

the synchrotron origin of the GeV radiation could be revealed by accurate modeling of the spectral and temporal behaviors of the broad-band gamma ray fluxes detected by *GLAST*, as well as by forthcoming ground-based Cherenkov detectors. Of particular interest in this regard could be the interpretation of flares which would *decline* rapidly at 0.1-1 GeV energies at the flare fading stage. The key observation here is that in FSRQs, the Compton radiation at these energies should be due to upscattering of external UV photons by electrons with $E' \lesssim 1$ GeV, which could have cooling times larger than the measured decline time, whereas the GeV synchrotron radiation is due to electrons with many orders of magnitude higher energies, and so it would have much shorter cooling times.

If radio galaxies are misdirected blazars and steep spectrum radio sources are off-axis FSRQs (Begelman, Blandford, & Rees 1984; Urry & Padovani 1995; Orr & Browne 1982), then the gamma-ray spectra of radio galaxies could also reveal hadronic acceleration in blazar jets. Nonthermal cosmic rays that escape from the inner jets of radio galaxies can accumulate in the central gas-rich region of the AGN. Nuclear collisions of these cosmic rays with ambient gas would produce a quasi-stationary (on time scales of thousands of years) and compact gamma-ray halo with a characteristic π^0 -decay feature near $70/(1+z)$ MeV. Note also that the bremsstrahlung emission from π^\pm -decay electrons of ~ 0.1 -1 GeV energies is likely to conceal the 70 MeV benchmark (Schlickeiser 1982). Nuclear interactions will give secondary π -decay emission that is brightest in the central BLR core of a radio galaxy where the target particle density is highest, and dimmer in the extended region due to the tenuousness of the interstellar medium on scales of hundreds of pc. Because of the rather small size of this hadronic halo, the gamma-ray detectors would detect it as a point source. Such a compact hadronic halo could be still resolved in the radio band, where the radio flux produced by secondary electrons of GeV energies would show an increase in brightness towards the center of the AGN on the milliarcsecond scale.

Considering possible signatures of relativistic hadrons during the flares, we note that a pronounced 70 MeV π^0 -decay maximum should be due first of all to hadrons with kinetic energies ~ 1 -10 GeV; therefore it would imply a mass-loaded jet. As we show in the Appendix A, the mass-loaded jet models are rather unlikely because they confront severe energetics difficulties. Nevertheless, the hadronic π^0 -decay gamma-ray feature, although significantly broadened and Doppler-shifted, could be expected in those particular cases when the inner jet dumps its energy in collisions with the dense target, such as a broad line cloud crossing the jet. Observations of radio galaxies with imaging X-ray telescopes, *GLAST*, and ground-based air Cherenkov telescopes with low energy thresholds will provide spectral data that should be analyzed for evidence of nonthermal hadrons in light of these considerations.

4.2. Neutrinos from FSRQs and BL Lacs

Detection of neutrinos from blazars will provide the most compelling evidence for hadronic acceleration in blazar jets. For photohadronic jet models, we have argued here and elsewhere (Atoyan & Dermer 2001) that the presence of a strong UV accretion-disk radiation field is required for blazar neutrino fluxes to be detectable with km-scale high-energy neutrino telescopes. The disk radiation field is needed to produce a quasi-isotropic scattered radiation component produced in the BLR of FSRQs. The existence of an external radiation field in FSRQs is suggested by luminous broad emission lines detected from these objects. For UV fields expected from optically-thick accretion disks, photomeson interactions can efficiently extract the energy of relativistic protons with (relatively modest) energies $\gtrsim 10^{15}$ eV, resulting in the production of neutrinos with $E_\nu \gtrsim 3 \times 10^{13}$ eV. For flares like the one detected in February 1996 from 3C 279 with EGRET, the fluence of neutrinos shown in Fig. 3 is at the level of 10^{-4} erg cm $^{-2}$, implying $\approx 0.3 \nu_\mu$ per flare (i.e., a detection probability of $\approx 30\%$). This would suggest a realistic possibility for IceCube to detect a few to several neutrinos from several flares over the course of a year. Given the flaring duty cycle of FSRQs estimated from EGRET observations ($\sim 10\text{-}20\%$), this implies that a few high-energy neutrinos will be detected from FSRQs such as 3C 279 on a time scale of 1 year. Considerably more will be detected if the efficiency to accelerate hadrons exceeds our baseline assumption given by equating proton and gamma-ray power. The additional possibility that some neutrinos will also be detected during quiescent states strengthens our prediction that FSRQs will be detectable high-energy neutrino sources with km-scale neutrino telescopes. We note that on a 1 year observation time scale, detection of only two neutrinos with energies above 30 TeV from the same direction pointed to a known blazar would represent a very significant detection of an astrophysical source, because at these energies the background cosmic-ray induced neutrino flux expected within one square degree (which is typical for the angular resolution of a high-energy neutrino telescope in ice or water) is $\lesssim 0.03$ (Gaisser, Halzen, & Stanev 1995).

For BL Lac objects, where the accretion-disk and scattered radiation components are much weaker, and with GeV gamma-ray fluxes that are also typically not as bright as in FSRQs, the chances for detection of neutrinos even with a 1 km-scale neutrino detector are negligible. For the proton fluxes shown in Figs. 6 and 7 calculated for parameters of the April 1997 flare in Mrk 501, the probability of neutrino detection during the flare is less than 10^{-6} . It is also important to note that unlike the case of $p\gamma$ interactions with the internal synchrotron photons, the intensity of $p\gamma$ interactions with the external radiation does not depend on the blob size. Therefore in FSRQs the neutrino production from photomeson interactions with the external radiation field does not decline so much in the process of expansion of the blob as it propagates through the quasi-isotropic external radiation field at

$R \lesssim R_{BLR}$ as it does in BL Lac objects. We note that the blob expansion seems unavoidable because of the difficulty in confining the high internal pressures of the blob by the pressure of the external medium.

An important issue concerns the quenching of the jet as it sweeps up mass from the BLR. As BLR clouds execute Keplerian rotational motion about the central supermassive black hole, some will pass through the path of the jet outflow. This will cause energization and deceleration of the radiating plasma, as in the external shock model of gamma-ray bursts (Mészáros & Rees 1993). Suppose that the AGN jet is beamed into a fraction $f_b = 0.01f_{-2}$ of the full sky. In a simple model with a uniform BLR gas density n_{BLR} within a spherical BLR with Thomson depth $\tau_T = n_{BLR}\sigma_T R_{BLR}$, the total mass in the beaming cone is $M_j(< R_{BLR}) \cong 5250f_b\tau_T R_{18}^2 M_\odot$, where $R_{18} = R_{BLR}/10^{18}$ cm (see Blandford & Levinson (1995) for BLRs with radially dependent densities). The time for BLR material to pass through the cone of the jet with opening half-angle $\theta_j \cong 2\sqrt{f_b}$ is $t_j \cong 1.1 \times 10^9 f_{-2}^{1/2} R_{18}^{3/2} / M_9^{1/2}$ s, where the mass of the central supermassive black hole is $M_9 = M_{bh}/10^9 M_\odot$. Assuming that the directional power of relativistic plasma expelled in the AGN jets is comparable to the apparent isotropic gamma-ray luminosity L_γ , then the flow will be significantly decelerated when $L_\gamma t_j \cong \Gamma^2 M_j(< R_{BLR}) c^2$, where Γ is the Lorentz factor of the plasma outflow. Thus, unless the mean apparent isotropic luminosity exceeds

$$L_\gamma(\text{ergs s}^{-1}) \cong 10^{48} (f_{-2} R_{18} M_9)^{1/2} \left(\frac{\tau_T}{0.1}\right) \left(\frac{\Gamma}{10}\right)^2, \quad (23)$$

the jet will be quenched by sweeping up BLR gas. This quenching process could make it difficult to form extended relativistic jets on the 10-100 kpc scale, as it may be required to explain enhanced X-ray emission in the knots of PKS 0637-752 (Tavecchio et al. 2000). The transport of inner jet energy to the extended jets via neutral beams avoids this difficulty. The neutrons and gamma-rays will pass through the BLR material without attenuation unless the Thomson depth of BLR is very high, with $\tau_T \gtrsim 10$. In these cases the jet and neutral beam outflow would be quenched, the nonthermal radiation would be reprocessed into lower energy emissions, and only the neutrino signal would penetrate through the dense inner region without reprocessing. If so, the neutrino emission from such buried jets in non-blazar sources could reveal these types of AGN. We return to this speculation in Section 4.4.

4.3. Energy Transport to the Extended Jet by Neutral Beams

Relativistic neutrons produced by $p\gamma$ collisions in the compact inner jet are no longer confined by the jet's magnetic field, and so can escape from the blob unless the neutron decays or interacts with another soft photon that results in conversion to a proton inside

the blob. Our calculations show that in FSRQs with luminous external radiation fields, up to $\sim 30\%$ of the total energy injected into the blob in the form of relativistic protons with $E \gtrsim 10^{15}$ eV can leave the blob in the form of relativistic neutrons with Lorentz factors $\gamma_n \gtrsim 10^6$.

For the case of FSRQs, neutrons escaping the inner blob continue to propagate in the BLR with its quasi-isotropic scattered accretion-disk radiation up to distances $R \sim R_{BLR} \sim 0.1\text{-}1$ pc. Subsequent interactions of the neutron beam with the scattered disk photons will result in the production of beamed secondaries. Neutrino secondaries will add to the overall neutrino flux. Importantly, a beam of gamma-rays with energies above 10^{15} eV is also produced. Because these gamma-rays are made outside the blob and propagate radially outward in the blob's frame, they do not interact with the internal synchrotron photons, and therefore have a chance to escape from the central region of the quasar (see Fig. 2). Depending on the extent and intensity of the isotropic external radiation field, as much as several per cent of the accelerated proton energy $W_p (\geq 10^{15}$ eV) injected in the inner jet at distances $R \leq R_{BLR}$ could thus be converted to gamma-rays which escape from the BLR.

Fig. 8 shows the mean-free-path of gamma rays due to pair-production interactions with photons of the diffuse cosmic microwave background radiation for $z = 0$ (solid curve) and $z = 0.538$ (dashed curve). This calculation also takes into account the diffuse extragalactic infrared radiation field. We approximate this field by a spectrum $\nu J_\nu \propto \text{const}$ at the level of total energy density $u_{IR} = 0.01$ eV cm $^{-3}$ between 0.001 mm and 1 mm (e.g., Primack et al. 1999), though the precise value is not important on the size scales $\lesssim 1$ Mpc under consideration.

Our calculations show that more energy is typically carried out from the BLR by relativistic neutrons than by gamma rays. This is especially true if the degradation of the neutron beam escaping the blob but still in the BLR is not very strong, which will always be the case for neutrons escaping the blob at distances $R \sim R_{BLR}$. The energy carried away by neutrons with $E_n \geq 10^{17}$ eV may reach $\sim 10\%$ of $W_p (\geq 10^{15}$ eV) for accelerated protons with number index $\alpha_p \simeq 2$. Adding the energy of the gamma rays to this, we find that $\sim 5\%$ can be used as a rough estimate for the fraction of total (starting from 1 GeV) energy of accelerated protons in the inner jet that is carried by the collimated beam of UHE neutrons and gamma rays to $>\text{kpc}$ distances in FSRQs.

For a flare like the one in February 1996 from 3C 279, the gamma-ray fluence measured with EGRET corresponds to an apparent isotropic energy release of 2×10^{54} erg. Assuming that the injection power in nonthermal protons in the inner jet is the same as for the parent electrons, the overall total energy in the neutral beam emerging from the inner jet per a single such flare could reach the level $\sim 10^{51} \delta_{10}^{-2}$ erg in the stationary frame. This energy will be

collimated in the cone with opening angle $\sim 1/\delta$, and it will be deposited at distances up to 0.1-1 Mpc, provided that the spectra of ultra-high energy neutrons extend up to 10^{19} - 10^{20} eV, as in Fig. 4b.

After neutron-decay or gamma-ray attenuation, the charged particles emerging in the direction of the parent neutral beam will interact with the ambient extragalactic medium via local magnetic and photon fields. In the case of the neutrons, a small fraction $\sim m_e/m_p$ of the neutron energy will appear in the form of β -decay electrons with Lorentz-factors $\gamma > 10^8$. This energy will be immediately available for radiation in the synchrotron and Compton processes with νF_ν peaks at hard X-ray and multi-TeV energies, respectively, for a 1 μ G field and a dominant local CMB radiation field (Dermer 2002). The dominant fraction of the initial neutron energy remains, however, in the protons. In order for the energy transport by the neutrons to be efficient from the point of view of powering the extended jets in radio galaxies, there should be a mechanism for effective transfer of the neutron-decay proton energy into the form of relativistic electrons.

Such a mechanism is expected through interactions of the relativistic protons as well as the e^+e^- pairs from the gamma-ray beam with the ambient magnetic field in the surrounding medium. In the case of a significant transverse magnetic field component B_\perp , both the protons and leptons will change their initial directions on the Larmor timescales $t_L = E/eB_\perp c$, which implies that a significant fraction of their momenta $p = E/c$ will be transferred to the ambient medium. Another, and possibly even more effective way for transferring the initial momentum and energy of the charged particles is by generating MHD turbulence through beam instabilities excited by the highly beamed neutron-decay protons and charged secondaries emerging from the charge-neutral beam. The continuous transfer of momentum and energy from the beam to the intergalactic medium could stretch the ambient magnetic field to form a channel facilitating beam propagation, or drive the medium into relativistic motion in the forward direction to create a powerful relativistic shock.

In the latter scenario, relativistic shocks can accelerate ambient electrons (as well as protons), thereby injecting a power-law electron spectra $Q_e(E) \propto E^{-\alpha}$ with $\alpha \geq 2$ in the downstream region. Synchrotron radiation from these electrons could then explain (Dermer and Atoyan 2002) the broad-band nonthermal radio, optical, and X-ray emission from hot spots and knots in the extended X-ray jets of extragalactic jet sources observed with the *Chandra Observatory*. The idea that the observed X-ray jets might be due to propagation of a powerful beam of gamma rays has also been considered by Neronov et al (2002) (see also Dermer & Li 2001), who suggested a “non-acceleration” scenario, where the observed X-rays could be due to synchrotron radiation from electrons formed in the electromagnetic cascade initiated by ultra-high energy gamma rays. Our calculations show that although

some contribution to the observed X-ray fluxes from the cascade electrons is not excluded, the spectral features of the observed radiation, in particular, X-ray energy spectral indices $\alpha_X \geq 1$, might be difficult to explain in a pure cascade scenario. Moreover, interpretation of the radio and optical fluxes from the same X-ray knots apparently makes unavoidable the requirement of in-situ acceleration of electrons in the X-ray knots. Given the total energy released by the neutrons and gamma rays per single flare, the energetics of these kpc-scale knots could be explained by superposition of jet activity on time scales up to thousands of yrs (since 1 kpc translates to $\simeq 3 \times 10^3$ yr of light travel time). Thus, the bright knots might represent the observable signatures of the past history of activity of the central engine of the blazar when powerful acceleration of UHE cosmic rays had occurred in the inner jets of the source.

Considering now the BL Lac objects, we note that in the case of weak or negligible external radiation field components, any significant transport of the inner jet energy by ultra-high energy gamma-rays in those objects is practically absent. This is because gamma-rays are not produced through $n\gamma$ interactions of the neutrons outside the compact blob, whereas the ultra-high energy gamma-rays produced in $p\gamma$ collisions inside the blob will be absorbed due to $\gamma\gamma$ collisions with the same internal synchrotron target photons (recall that $\sigma_{\gamma\gamma} \gg \sigma_{p\gamma}$). Nevertheless, up to $\sim 10\%$ of the energy injected into the inner jet in relativistic protons with $E > 1$ PeV could still be taken out of the blob by neutrons with $E \gtrsim 10^{17}$ eV due to $p\gamma$ collisions with synchrotron photons while the blob remains compact. Because of the latter limitations, and because BL Lac sources are generally much less powerful than FSRQs, the total energy that the neutron beam can extract from the accelerated protons is much less for BL Lacs than for FSRQs. Moreover, because of the smaller sizes and magnetic fields inferred for BL Lac objects, the level of neutron production and the maximum energy of accelerated protons is reduced in the former class of sources. Thus the neutral beam power is much less in BL Lac objects than in FSRQs.

4.4. Explanation of Observed Features of Radio-Loud Active Galactic Nuclei

As a consequence of processes occurring in the inner jets of blazars, we predict that powerful collimated neutral beams that extend as far as hundreds of kpc from the nucleus are ejected in the axial jet directions in high luminosity FSRQs. The linearity and the spatial extent of the ejecta is a consequence of the decay properties of the neutrals. This process can explain the origin of X-ray jets detected by *Chandra*, which appear straight on scales of up to Mpc, such as the jet in Pictor A (Wilson, Young, and Shopbell 2001). The linearity of the radio jets in Cygnus A (Perley, Dreher, & Cowan 1984) may also be a consequence of

energetic neutral beams powering the lobes of powerful FR II galaxies. This interpretation avoids firehose instabilities in models invoking magnetic fields to collimate the extended FR II radio jets, or problems associated with jet quenching, as discussed in Section 4.2.

Our model predicts that lower luminosity blazars, in particular, the lineless BL Lac objects, have orders-of-magnitude weaker neutral beams than FSRQs. The maximum energies of the relativistic neutrons are also about an order-of-magnitude less in Mrk 501-like BL Lac objects than in 3C 279-like FSRQs. Consequently the X-ray jets driven by the high-energy neutron beams will be generally fainter (despite their relative proximity) and shorter in BL Lac objects. This could explain the faint kpc-scale X-ray jets detected from objects like 3C 371 (Pesce et al. 2001), which is an off-axis BL Lac object (Miller 1975).

We adopt the point of view, following Urry & Padovani (1995), that FR I and FR II galaxies are the parent populations of BL Lac objects and FSRQs, respectively. The less powerful beams of neutrons that occupy smaller spatial scales in BL Lac objects compared to FSRQs conforms to the measured relative power requirements in FR I and FR II galaxies (Fanaroff & Riley 1974). If FR I/BL Lacs have smaller Lorentz factors than FR II/FSRQs, as also inferred from observations of these sources (Urry & Padovani 1995), then the weak, broad twin-jet morphologies in FR I galaxies can be qualitatively understood. We point out that even though the inner parsec regions of a BL Lac are much less dense than the BLRs in FSRQs in view of their relative emission line strengths, the jet quenching problem (Section 4.2) can still be severe for BL Lac objects because of their weaker jets.

The transport of energy by neutral particles to the extended jet will be enhanced by an intense external radiation field in the inner regions of the jet. The total power into the jet depends foremost on the accretion rate, which depends on the amount of gas and dust available to fuel a supermassive black hole. Thus our model is consistent with the evolutionary scenario proposed by Böttcher & Dermer (2002) and Cavaliere & D’Elia (2002) to explain the spectral sequence of FSRQs, and low- and high-frequency peaked BL Lac objects. According to this picture, FSRQs evolve into BL Lac objects due to a reduction in the accretion rate of the surrounding dust and gas that fuels the central black hole. (Note, however, that the jet power is derived primarily from mass accretion in the scenario of Böttcher & Dermer (2002) and from the spin energy of the black hole in the scenario of Cavaliere & D’Elia (2002).) Maraschi & Tavecchio (2002) argue that this picture accounts for the correlation between the radio jet and accretion power, where the latter is inferred from emission line strengths. High-energy neutrino observations will be crucial to test this scenario, as neutral beams of high energy neutrons and gamma-rays will be made in association with high-energy neutrinos. Finally we speculate that if ultraluminous infrared galaxies and quasars evolve into radio-loud AGNs (Sanders et al. 1988), then some ultraluminous infrared galaxies could

harbor buried jet sources that will be revealed through their high-energy neutrino emission.

4.5. Summary

Production of narrow beams of ultra-high energy neutrons with $E \geq 10^{17}$ eV becomes possible if relativistic compact jets of blazars accelerate cosmic rays to these energies. Such neutral relativistic particle beams can be especially powerful in FSRQs, where the neutrons are efficiently produced in $p\gamma$ interactions with photons of the external quasi-isotropic radiation field on timescale of years (since the broad-line region size scale $R_{BLR} \sim 0.1\text{-}1$ pc). In radio-loud jet sources, the beam could contain a significant fraction of ultra-high energy gamma-rays produced in the BLR through $n\gamma$ photomeson interactions by neutrons which escape from the compact relativistic plasma blob that forms the inner jet. These charge-neutral beams of UHE neutrons and gamma-rays (including also neutrinos which, however, do not contribute to the process of energy transport) do not interact with the extragalactic medium until either the neutrons decay or the gamma rays collide with soft photons on scales from kpc to Mpc. The main soft-photon target for $\gamma\gamma$ collisions is provided by the CMB radiation and, in some sufficiently powerful sources, also by low-frequency synchrotron radiation self-produced along the jet (Neronov et al 2002).

The weaker neutral beams in FR I radio galaxies and BL Lac objects, compared to FR II radio galaxies and FSRQs, could explain the morphological differences between the two classes of radio galaxies. This scenario assumes that the inner jets of blazars are effective accelerators of high-energy cosmic rays. The limits on acceleration that we consider do not preclude the acceleration of cosmic rays to energies $\gtrsim 10^{20}$ eV in blazars, especially in the more luminous FSRQs. This mechanism of relativistic energy transport from the central engine of AGN to large distances avoids problems of jet quenching in the central gas-rich regions of AGN, problems of adiabatic and radiative losses, and problems of long-term confinement and stability (on scales up to 10^6 yr) of the jet against different plasma processes. Beam instabilities can, however, provide an effective method to transfer the energy of ultra-relativistic protons emerging from the neutron beam into the surrounding medium, and driving relativistic shock which ultimately accelerates nonthermal electrons to radiate observable synchrotron and Compton emission. Given also the large amount of energy that such a beam may contain, which can be of the order of a few percent of the inner jet power, our results suggest that the detection by the *Chandra Observatory* of the narrow X-ray jets that remain straight on scales beyond several hundreds of kpc provides observational evidence that the relativistic inner jets of blazars, first of all the flat spectrum radio quasars, are powerful accelerators of UHE cosmic rays. Detection of high-energy neutrinos from

FSRQs with IceCube or a Northern Hemisphere high-energy neutrino telescope will provide strong support for this scenario.

We thank Hui Li for discussions about the physics of jets. AA appreciates the hospitality and support of the NRL High Energy Space Environment Branch during his visit when this work has been done. The work of CD is supported by the Office of Naval Research and NASA grant No. DPR S-13756G.

A. Comparison of Mass-loaded and Photopion Hadronic Jet Models

Relativistic neutrons are produced with $\sim 50\%$ probability in the inelastic collisions of relativistic protons either with an ambient thermal proton or with a photon above the photopion production threshold. However, the mass-loaded jet models, i.e. the ones invoking pp nuclear collisions, can be practically excluded on the basis of efficiency arguments. As equation (1) shows, nuclear interactions could provide energy loss time scales shorter than the dynamical time $t'_{dyn} = R'/c$ only if the source is very thick to Thomson scattering, $\tau_{sc} > 40$. If one requires that, say, non-thermal X-ray flux are produced during the flare, i.e. $\tau_{sc} < 1$, then the observed fast decline of the fluxes could be attributed to the adiabatic losses of proton energy and fast decline of the gas density on dynamical time scale due to rapid expansion of the source. However, the overall energy losses of protons in nuclear interactions during that time cannot exceed $\simeq 2.5\%$. In practice it means that the real power injected into the blob in the form of relativistic protons should be by a factor of $\gtrsim 100$ larger than the power inferred from the observed radiation fluence.

Besides these inefficiency problems, a serious argument against hadronic nuclear interaction models is that the mass-loaded jets would require too great a total energy in the blob including the kinetic energy. Thus, for a blob size $R' \sim t_{var}c\delta/(1+z)$ with typical $t_{var} \simeq 1$ d and $\delta \simeq 10$ the Thomson scattering depth $\tau_{sc} = 1$ implies a gas density (in terms of 'H-atoms', and omitting here the dependence on the source redshift z) $n_H \sim 6 \times 10^7 \text{ cm}^{-3}$. The jet mass then is $M_j \simeq 3.5 M_\odot$, and the kinetic energy $W_{kin} = (\Gamma - 1)M_jc^2 \sim 6 \times 10^{55} \text{ erg}$ for $\Gamma \simeq \delta \sim 10$. Thus, even such a jet with reduced efficiency should have a significant mass load leading to an unacceptably high energetics required in a single blob. One might suppose that it would be possible to bring the kinetic energy requirements down to a formally acceptable values by reducing further the density of the gas. However, then the total energy of relativistic protons W_p in the blob should be increased in order to provide a given level of radiation fluxes by pp -interactions.

Indeed, the integral luminosity of the radiation that could be produced in pp -interactions,

is given by $L'_r \simeq \eta_r W'_p / t'_{pp}$, where η is the fraction of relativistic proton energy that goes to secondary electrons and gamma-rays. Assuming that most of the electron energy will be processed to electromagnetic radiation, we can have $\eta \cong 0.5$, leaving the rest for the neutrinos. Transforming from the blob frame to the observer (or stationary) frame, the total energy $W_{\text{tot}} = W_p + W_{\text{kin}}$ can be written as

$$W_{\text{tot}} \simeq 4\pi\Gamma m_p c^2 \left[\frac{4d^2 f_{\text{tot}} (1+z)^4}{\sigma_{pp} m_p c^3 \delta^4} (n'_H)^{-1} + \frac{(t_{\text{var}} c \delta)^3}{3(1+z)^3} n'_H \right], \quad (\text{A1})$$

where f_{tot} is the total energy flux, i.e. $\int F(\nu) d\nu$ which is typically larger than the $\nu F(\nu)$ that a model is intended to explain. Here we have assumed for the kinetic energy $(\Gamma - 1)/\Gamma \simeq 1$, and substituted $K_{pp} = 0.5$ for the inelasticity. The energy W_{tot} reaches a minimum at the density

$$n'_{H,\text{min}} \simeq 2.25 \times 10^9 d_{28} f_{-10}^{1/2} t_{\text{var}}^{-3/2} (d) \delta^{-7/2} (1+z)^{7/2} \text{ cm}^{-3}, \quad (\text{A2})$$

where $f_{-10} \equiv f_{\text{tot}}/10^{-10} \text{ erg cm}^{-2} \text{ s}^{-1}$, and $d_{28} \equiv d/10^{28} \text{ cm}$. The minimum of W_{tot} is then

$$W_{\text{min}} \simeq 1.6 \times 10^{54} d_{28} f_{-10}^{1/2} t_{\text{var}}^{3/2} (d) \delta_{10}^{1/2} (1+z)^{-1/2} \text{ erg}. \quad (\text{A3})$$

Here $\delta_{10} \equiv \delta/10$, and we have assumed $\Gamma = \delta$ in equation (A1). Interestingly, W_{min} is reached when the kinetic and internal CR energies become equal. Note that any noticeable deviation of the real density in the jet from $n_{H,\text{min}}$ required for W_{min} will immediately increase further the total energy requirement given by equation (A1).

A hadronic nuclear interaction jet model which would like to make any significant contribution to the fluxes of flares observed by EGRET from FSRQs, like the 1996 flare of 3C279, would have to assume an absolute (in the stationary frame) energy in a single flare exceeding by orders of magnitude an energy of a supernova explosion. Even for a less powerful but much closer blazars, like BL Lac objects Mrk 421 or Mrk 501, any significant contribution to the total radiation flux from mass-loaded nuclear interaction jet models can be practically excluded. Indeed, even taking into account that the variability timescale might be as short as 1 h instead of 1 day, for interpretation of the maximum fluxes at the level of $f_{\epsilon} \simeq 10^{-9} \text{ erg cm}^{-2} \text{ s}^{-1}$ the minimum energy W_{min} would still significantly exceed the ‘supernova’ level 10^{51} erg , which is problematic to accept for these objects with a relatively modest average bolometric luminosities. The only type of relativistic extragalactic sources for which the hadronic nuclear interaction models could still be reasonable from the general total-energy consideration seem GRB sources where variability timescale is very short (hence the densities could be very high) although the peak fluxes are much higher than for relativistic jets. Noticing that $f_{\text{tot}} \times t_{\text{var}}$ is actually a good estimate for the fluence Φ observed during the flare, we can re-write equation (A3) as

$$W_{\text{min}} \simeq 6.3 \times 10^{49} d_{28} \Phi_{-5}^{1/2} (t_{\text{var}}/1\text{s}) (\delta/100)^{1/2} (1+z)^{-1/2} \text{ erg},$$

where $\Phi_{-5} \equiv \Phi/10^{-5} \text{ erg cm}^{-2}$. Obviously, this is a reasonable value for GRB source, although the question on the efficiency of the pp -interaction model in case of simultaneous detection of non-thermal X-rays and gamma-rays should be still addressed.

B. Relative Importance of the Direct Disk and Scattered Radiation Fields for Photomeson Production

Equations (8) and (9) can now be used to estimate the relative importance of the photomeson interactions of relativistic nucleons with the direct and scattered components of the accretion disk radiation, respectively. For the direct disk radiation photon spectral density $n(\epsilon, \Omega) = u(\epsilon, \Omega; h)/\epsilon$, we analytically estimate the dimensionless number of photomeson collisions per unit path dh (in terms of gravitational radius R_g), $\kappa_{dir} = \nu_{p\gamma} R_g/c$, where the collision rate $\nu_{p\gamma}$ is given by an integral (2) without the inelasticity term $K_{p\gamma}$. This yields the simple formula

$$\kappa_{dir}(h, E) \approx 4.1 \times 10^3 l_{ad} \frac{I(h, E)}{h^{9/4}} \left(\frac{\epsilon_*}{100 \text{ eV}} \right)^{-1} \frac{\bar{\sigma}}{200 \mu\text{b}}. \quad (\text{B1})$$

Here $l_{ad} = L_{ad}/L_{Edd}$ is the total luminosity of the disk radiation in units of Eddington luminosity L_{Edd} , and

$$I(h, E) = \int \frac{1 - \cos \psi}{\tan^{9/4} \psi} d \cos \psi, \quad (\text{B2})$$

where the integration is to be performed only over the collision angles ψ satisfying the threshold condition

$$C(\psi) \equiv \frac{1 - \cos \psi}{\tan^{3/4} \psi} \geq \frac{\epsilon_{th} h^{3/4}}{\epsilon_* \gamma_{p,n}}, \quad (\text{B3})$$

with $\gamma_{p,n} = E/m_p c^2$ (for $m_n = m_p$) corresponding to the Lorenz-factor of the incident proton or neutron. For simplicity of the analytic estimate (B1), we here approximate the $p\gamma$ interaction cross section $\sigma(\epsilon_r)$ as a single step-function with a height $\bar{\sigma} \sim 200 \mu\text{b}$ between σ_1 and σ_2 , starting from the threshold energy $\epsilon_{th} \simeq 150 \text{ MeV}$.

A similar analytic estimate for the coefficient $\kappa_{iso}(E)$ is derived for the scattered quasi-isotropic component of the external radiation field (9). For distances $h \leq r_{BLR}$, i.e. inside the BLR with dimensionless radius r_{BLR} , this results in

$$\kappa_{iso}(E) \simeq 1.1 \times 10^5 \frac{l_{ad} \tau_T}{r_{BLR}^2} \left(\frac{\epsilon_{max}}{20 \text{ eV}} \right)^{-1} \frac{\bar{\sigma}}{200 \mu\text{b}}, \quad (\text{B4})$$

where $\epsilon_{max} = \epsilon_*/r_i^{3/4}$, with $r_i \geq 6$, as described above.

Because the scattered radiation is quasi-isotropic, the interaction threshold condition for photopion production in this field is the same at all heights $h < r_{BLR}$, and is defined by head-on collisions of protons and neutrons with photons with maximum energy $\epsilon \simeq \epsilon_{max}$. For $\epsilon_{max} \simeq 20$ eV, this requires nucleon energies $E > E_{th} \simeq 4 \times 10^6 m_p c^2$. Meanwhile, because of the follow-on collisions that nucleons, which are moving predominantly along the jet away from the black hole, make with the photons of the direct disk radiation field, the interaction threshold of the nucleons with this field significantly increases with increasing height h . From equation (B3), we find $E > E_{dir}(h) \simeq 4.5 \times 10^6 h^{3/4} m_p c^2$, taking into account that the function C_ψ reaches a maximum $\simeq 0.331$ at $\psi = 60^\circ$. This means that only particles with energies $E \gg 10^{17}$ eV have effective interactions with the direct disk radiation component once the jet reaches heights $h \gtrsim 100$. Meanwhile, interactions of *all* particles with energies above 4 PeV can effectively continue until heights $h \simeq r_{BLR} \sim 2 \times 10^3$ - 10^4 (corresponding to $R_{BLR} \sim 0.1$ - 1 pc for a black hole mass $M_{bh} \sim 10^9 M_\odot$).

The characteristic photomeson opacity $\tau_{iso} \simeq \kappa_{iso} r_{BLR}$ due to interactions with BLR photons can be very significant for $l_{ad} \gtrsim 0.1$ and $\tau_T \sim 0.1$. For comparison, the characteristic photomeson opacity $\tau_{dir} = \kappa_{dir} h$ from the direct disk radiation field on scales h can be significant ($\gtrsim 1$) only rather close to the black hole, at $h < 100$. This applies only to particles well above the interaction threshold $E_{dir}(h)$, when the integration limits in the integral (B2) cover a significant fraction of the maximum allowed range $0 < \cos \psi < 1$, when $I(h, E)$ reaches a maximum about 0.25. Given these considerations, we consider only interactions with the quasi-isotropic (i.e, scattered BLR field) component of the external disk radiation. Note that the acceleration of nonthermal particles may occur at large distances from the central black hole if due either to collision of relativistic shells or to interactions of the outflowing plasma with ambient gas in the BLR.

REFERENCES

Atoyan, A. M. & Aharonian, F. A. 1996, MNRAS, 278, 525

Atoyan, A. M. 1992a, A&A, 257, 465

Atoyan, A. M. 1992b, A&A, 257, 476

Atoyan, A., & Dermer, C. D. 2001, Phys. Rev. Lett., 87, 221102

Beall, J. H. & Bednarek, W. 1999, ApJ, 510, 188

Bednarek, W., and Protheroe, R. J. 1999, MNRAS, 302, 373

Begelman, M. C., Rudak, B., and Sikora, M. 1990, ApJ, 362, 38

Begelman, M. C., Blandford, R. D., & Rees, M. J. 1984, Reviews of Modern Physics, 56, 255

Berezinskii, V. S. & Grigor'eva, S. I. 1988, A&A, 199, 1

Berezinskii, V. S. Bulanov, S. V., Dogiel, V. A. Ginzburg, V. I. and Ptuskin, V. S. 1990, Astrophysics of Cosmic Rays (North-Holland: Amsterdam), chpt. 4

Blandford, R. D. & Levinson, A. 1995, ApJ, 441, 79

Blumenthal, G. R., and Gould, R. J. 1970, RMP, 42, 237

Böttcher, M. & Dermer, C. D. 2002, ApJ, 564, 86

Böttcher, M. 1999, ApJ, 515, L21

Böttcher, M. 2000, in GeV-TeV Gamma Ray Astrophysics Workshop, ed. B. L. Dingus, M. H. Salamon, and D. B. Kieda (AIP: New York), p. 31

Catanese, M. et al. 1997, ApJ, 487, L143

Cavaliere, A. & D'Elia, V. 2002, ApJ, 571, 226

Celotti, A. & Fabian, A. C. 1993, MNRAS, 264, 228

Dermer, C. D., 2002, ApJ, July 20, 2002, 574, 65

Dermer, C. D., and Schlickeiser, R. 1993, ApJ, 416, 458 (DS93)

Dermer, C. D., & Schlickeiser, R. 2002, ApJ, 575, in press (astro-ph/0202280)

Dermer, C. D., Sturner, S. J. and Schlickeiser, R. 1997, *ApJS*, 109, 103

Dermer, C. D. 1995, *ApJ*, 446, L63

Dermer, C. D., & Li, H. 2001, in *Gamma 2001*, eds. S. Ritz, N. Gehrels, and C. R. Shrader (AIP:New York), 286

Dermer, C. D., and Atoyan, A. 2002, *ApJ*, 568, L81

Fanaroff, B. L. & Riley, J. M. 1974, *MNRAS*, 167, 31P

Gaisser, T. K., Halzen, F., & Stanev, T. 1995, *Phys. Rep.*, 258, 173

Gallant, Y. A. in “Relativistic Flows in Astrophysics”, ed. by A. W. Guthmann et al., (Springer Verlag-New York), in press (astro-ph/0201243)

Giovanoni, P. M. & Kazanas, D. 1990, *Nature*, 345, 319

R.C. Hartman et al. 1996, *ApJ*, 461, 698

Hartman, R. C., et al. 1999, *ApJS*, 123, 79

Hartman, R. C. et al. 2001, *ApJ*, 553, 683

de Jager, O. C., Harding, A. K., Michelson, P. F., Nel, H. I., Nolan, P. L., Sreekumar, P., & Thompson, D. J. 1996, *ApJ*, 457, 253

Kirk, J. G., and Mastichiadis, A. 1989, *A&A* 213, 75

Krawczynski, H., Coppi, P. S., Aharonian, F. 2002, submitted to *MNRAS* (astro-ph/0204229)

Lichti, G. G. et al. 1995, *A&A*, 298, 711

Mannheim, K. 1993, *Astron. Astrophys.* 269, 67

Mannheim, K., and Biermann, P.L. 1992, *Astron. Astrophys.* 253, L21

Maraschi, L., & Tavecchio, F. 2002, *ApJ*, in press (astro-ph/0205252)

Mastichiadis, A. & Kirk, J. G. 1997, *A&A*, 320, 19

Mészáros, P. & Rees, M. J. 1993, *ApJ*, 405, 278

Miller, J. S. 1975, *ApJ*, 200, L55

Mücke, Rachen, J.P., A., Engel, R., Protheroe, R.J., and Stanev, T. 1999, *Pub. Astron. Soc. Australia*, 16, 160

Mücke, A., Protheroe, R.J., Engel, R., Rachen, J.P., Stanev, T. 2002, *Astropart. Phys.*, in press (astro-ph/0206164)

Neronov, A., Semikoz, D., Aharonian, F., and Kalashev, O. 2002, *PRL*, submitted (astro-ph/0201410)

Netzer, H. 1990, in *Active Galactic Nuclei, Saas-Fee Advanced Course 20*, ed. T. J.-L. Courvoisier and M. Mayor (Springer-Verlag: New York), p. 57

Orr, M. J. L. & Browne, I. W. A. 1982, *MNRAS*, 200, 1067

Perley, R. A., Dreher, J. W., & Cowan, J. J. 1984, *ApJ*, 285, L35

Pesce, J. E., Sambruna, R. M., Tavecchio, F., Maraschi, L., Cheung, C. C., Urry, C. M., and Scarpa, R. 2001, *ApJ*, 556, 79

Pian, E. et al. 1998, *ApJ*, 492, L17

Pian, E. et al. 1999, *ApJ*, 521, 112

Pohl, M. & Schlickeiser, R. 2000, *A&A*, 354, 395

Primack, J. R., Bullock, J. S., Somerville, R. S., & MacMinn, D. 1999, *Astroparticle Physics*, 11, 93

Quinn, J. et al. 1999, *ApJ*, 518, 693

Sambruna, R. M. et al. 2000, *ApJ*, 538, 127

Sanders, D. B., Soifer, B. T., Elias, J. H., Neugebauer, G., & Matthews, K. 1988, *ApJ*, 328, L35

Schlickeiser, R. 1982, *A&A*, 106, L5

Schuster, C., Pohl, M., & Schlickeiser, R. 2002, *A&A*, 382, 829

Sikora, M., Błażejowski, M., Begelman, M. C., & Moderski, R. 2001, *ApJ*, 554, 1; (e) 2001, *ApJ*, 561, 1154

Sikora, M. 1997, in *the Fourth Compton Symposium*, ed. C. D. Dermer, M. S. Strickman, and J. D. Kurfess (AIP: New York), 494

Sikora, M., Begelman, M. C., and Rees, M. J. 1994, *ApJ*, 421, 153

Sikora, M., Begelman, M. C., and Rudak, B. 1989, *ApJ*, 341, L33

Shakura, N. I., and Sunyaev, R. A. 1973, *A&A*, 24, 337

Stanev, T., Engel, R., Mücke, A., Protheroe, R. J. & Rachen, J. P. 2000, *Phys. Rev. D*, 62, 093005

Stecker, F. W. 1968, *Phys. Rev. Lett.*, 21, 1016

Tavecchio, F., Maraschi, L., & Ghisellini, G. 1998, *ApJ*, 509, 608

Tavecchio, F. et al. 2001, *ApJ*, 554, 725

Tavecchio, F., Maraschi, L., Sambruna, R. M., & Urry, C. M. 2000, *ApJ*, 544, L23

Totani, T. 1999, *ApJ*, 511, 41

Urry, C. M., & Padovani, P. 1995, *PASP*, 107(715), 803

Weekes, T. C. 2001, in *High Energy Gamma-Ray Astronomy*, ed. F. A. Aharonian and H. J. Völk (AIP: New York), 15

Wehrle, A. E. et al. 1998, *ApJ*, 497, 178

Wilson, A. S., Young, A. J., and Shopbell, P. L. 2001, *ApJ*, 547, 740

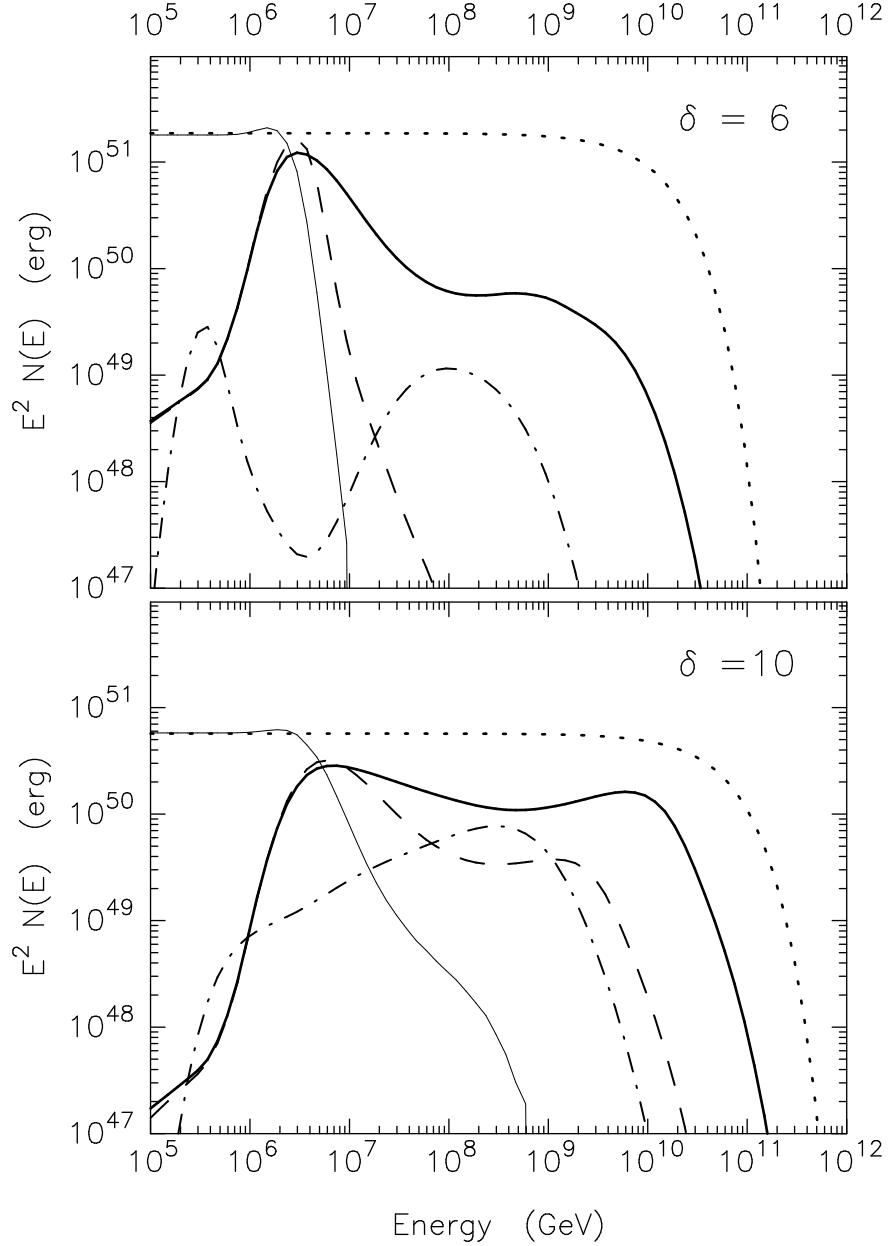


Fig. 1.— Spectra of protons injected into the blob (dotted curves), protons which remain in the blob when it reaches the edge of the BLR (thin solid curves), neutrons escaping from the blob (thick solid curves), and escaping neutrons (dashed curves) and gamma rays (dot-dashed curves) which reach the edge of the BLR for the cases of $\delta = 6$ and $\delta = 10$ in the upper panel (a) and lower panel (b), respectively. Model parameters relevant to the February 4-6 flare from 3C 279 detected by EGRET are used, as described in Section 3.1.

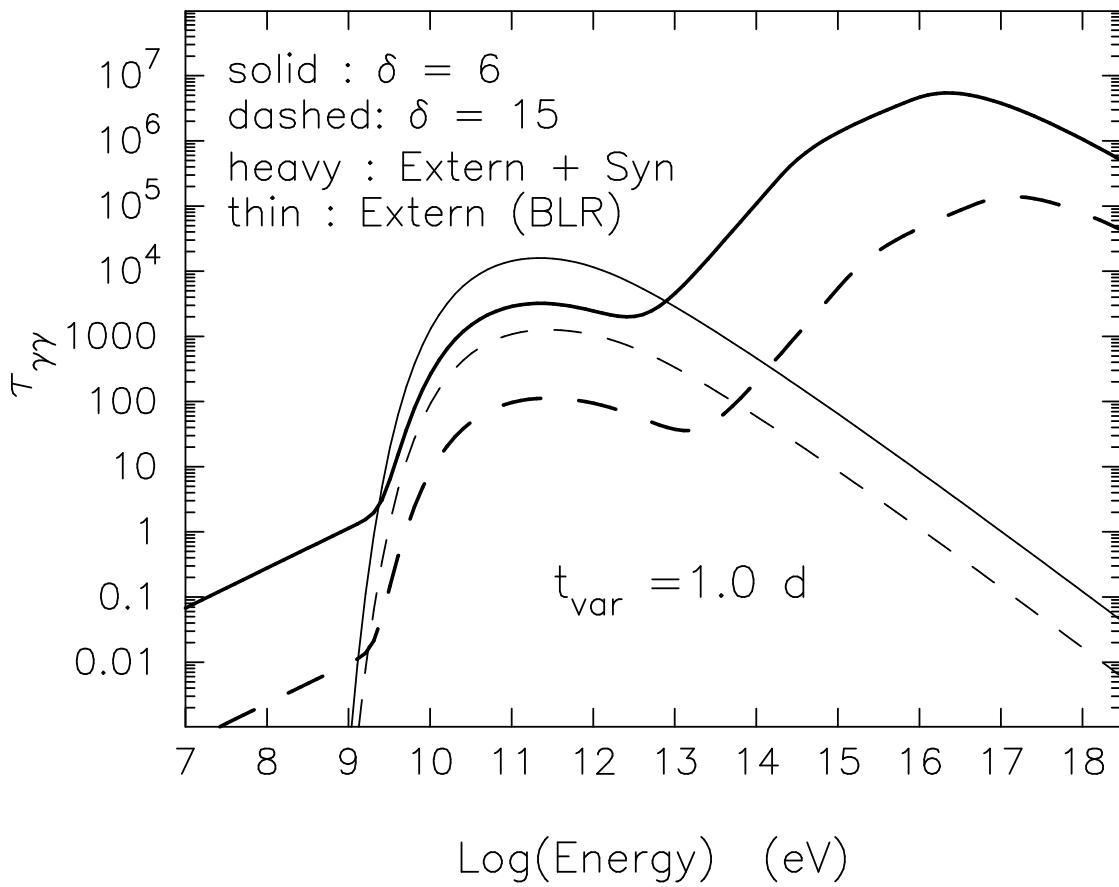


Fig. 2.— Pair production opacity due to $\gamma\gamma$ interactions inside the blob and in the BLR, as indicated in the figure legend.

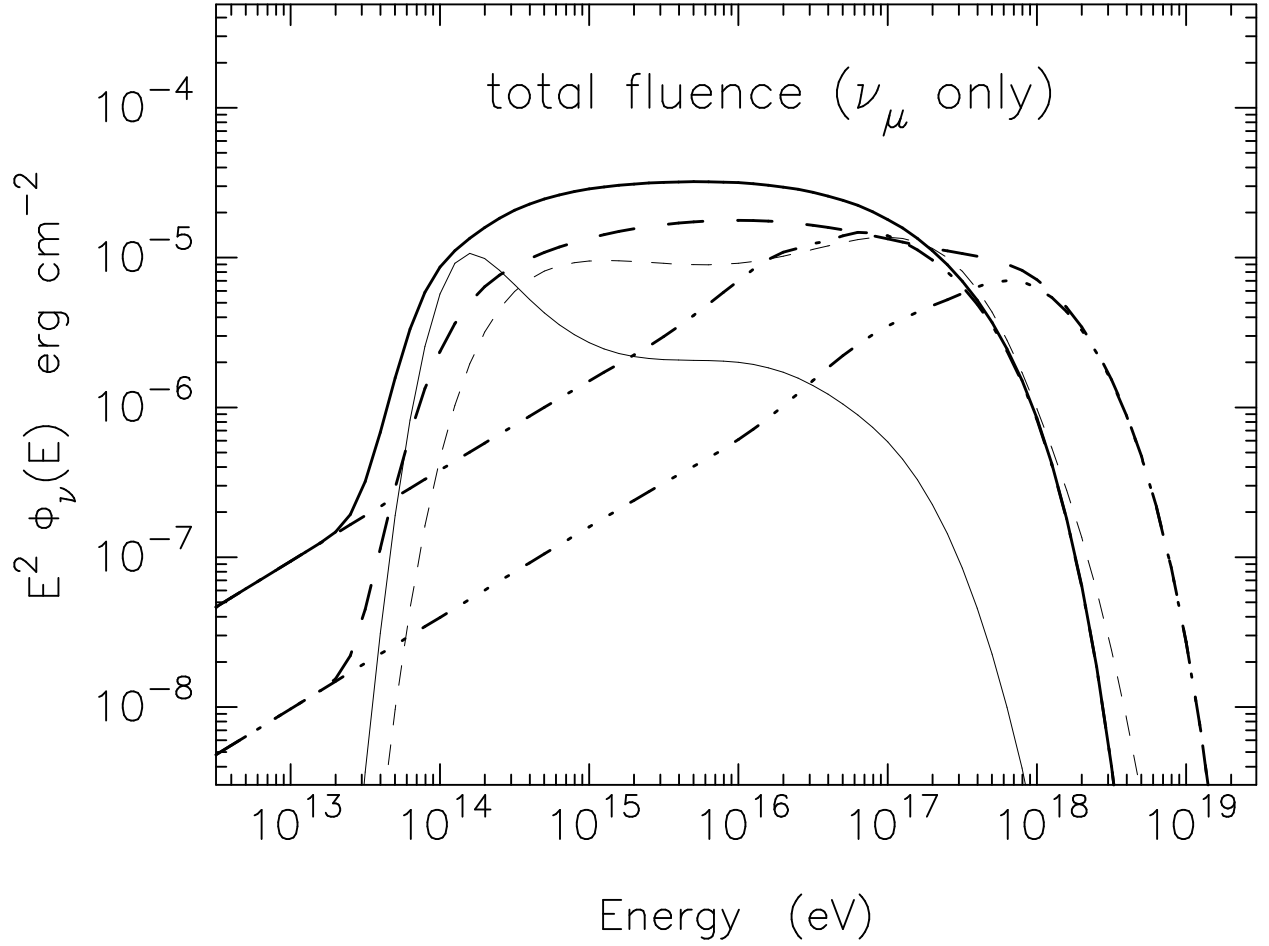


Fig. 3.— Fluences of neutrinos integrated over several days in the observer frame determined by the time for the blob to pass through the BLR, for the same parameters as used in Fig. 1. The solid and dashed curves show the fluences calculated for $\delta = 6$ and 10 , and the thick and thin curves represent the fluences of neutrinos produced by photopion interactions inside and outside the blob, respectively. The dot-dashed and 3-dot – dashed curves show the fluences due to $p\gamma$ collisions if external radiation field is not taken into account.

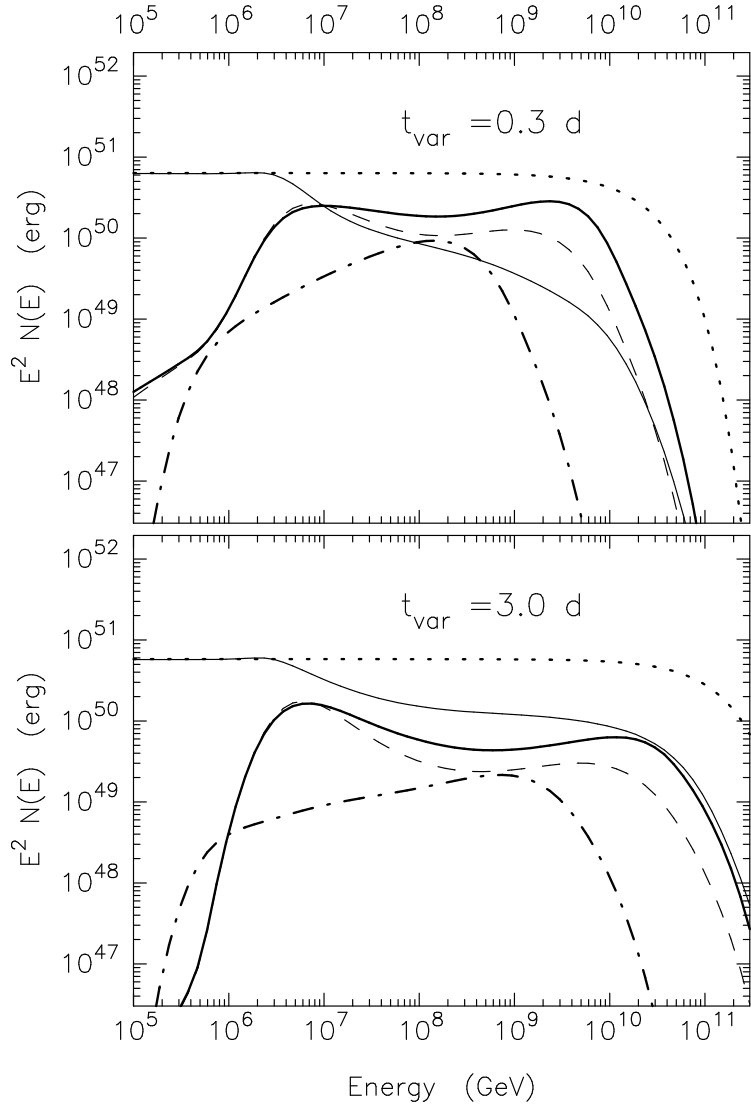


Fig. 4.— Spectra of injected protons (dotted curves), protons surviving when the blob reaches the edge of the BLR (thin solid curves), neutrons that escape from the blob (thick solid curves), neutrons (dashed curves) and gamma-rays (dot-dashed curves) that reach the edge of the BLR without attenuation for the same overall parameters as used in Fig. 1 for $\delta = 10$, but calculated assuming different sizes of the blob, corresponding to $t_{var} = 0.3$ and 3 days in the upper and lower panels, respectively. In calculation here we assume also that the same amount of accelerated protons as in Fig. 1 is now injected continuously during the entire time of passage of the jet through BLR, $t_{inj} = 7.9$ d in the observer frame, instead of $t_{inj} = 2$ d in Fig. 1.

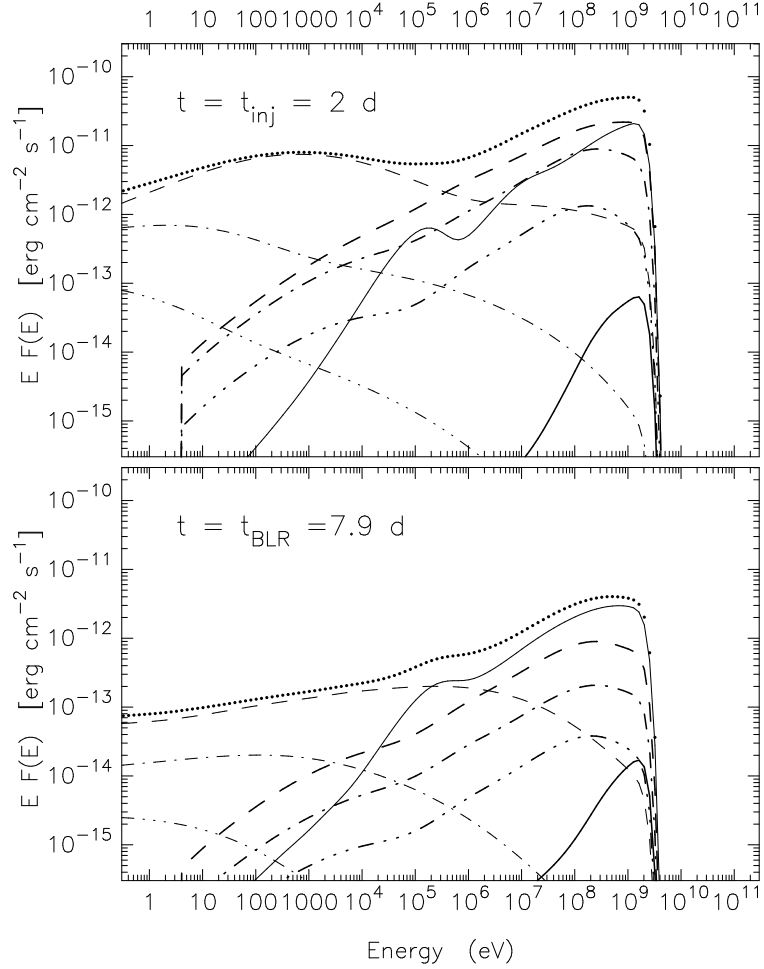


Fig. 5.— Radiation flux produced in and escaping from the blob (full dots) following the electromagnetic cascade initiated by energetic electrons and gamma rays produced in photo-pion interactions for the case $\delta = 10$ and the model parameters as in Fig. 1. The thick and thin curves correspond to synchrotron and Compton scattered radiation, respectively. The radiation of the first generation of electrons, which includes both the electrons from π^\pm decay and the electrons produced by absorption of π^0 -decay gamma rays in the blob, are shown by the solid curves. The dashed, dot-dashed and 3-dot-dashed curves show contributions from the 2d, 3d and 4th generations of cascade electrons, respectively. The upper and lower panels (a) and (b) show the cascade radiation flux at $t = 2d$, when injection of accelerated protons stops, and at $t = 7.9$ d, when the blob leaves the BLR, respectively.

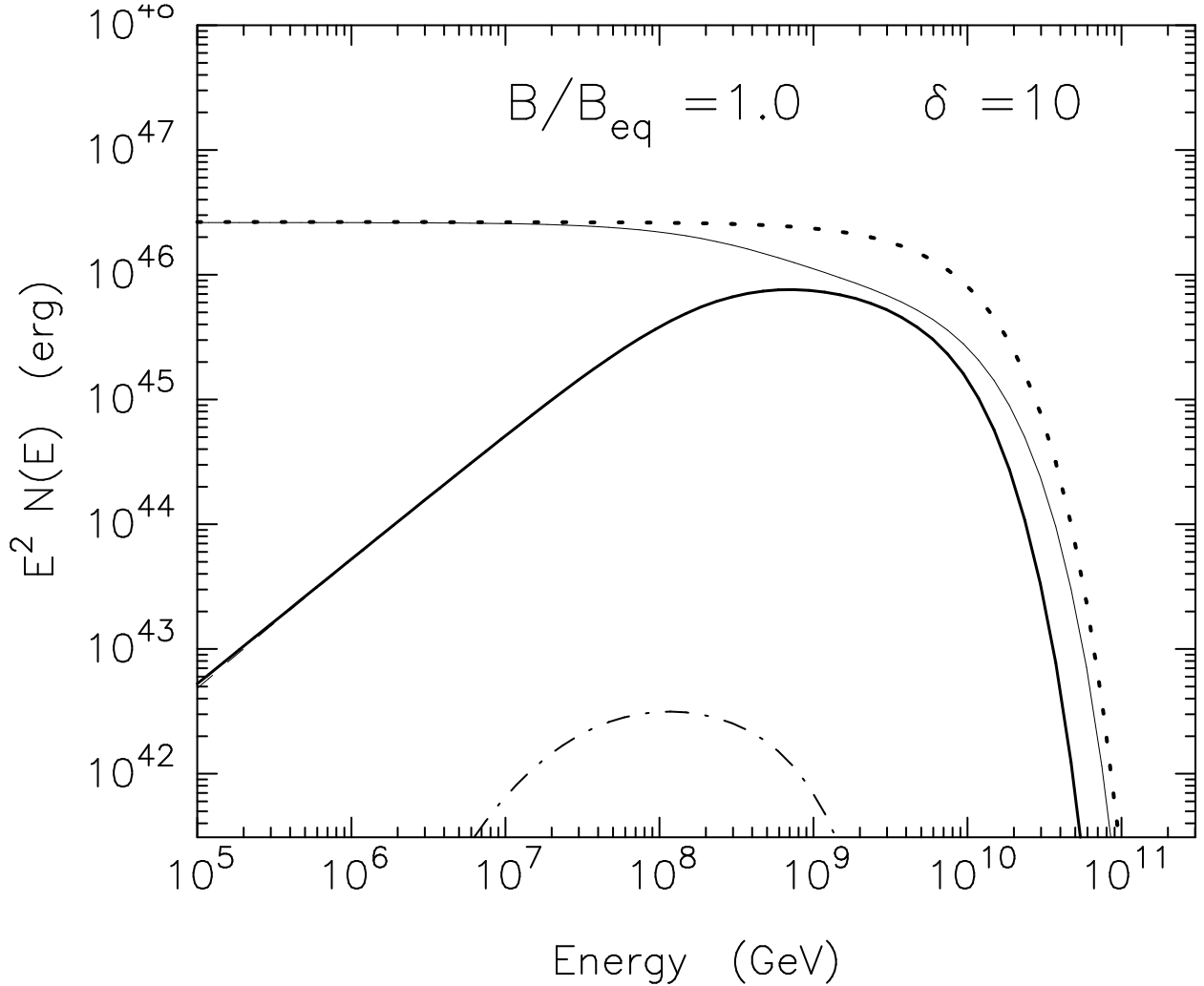


Fig. 6.— Total energy spectra of injected protons (dotted curve), and protons remaining in the blob (thin solid curve) at the time when the jet, with model parameters relevant to the April 1997 flare from Mrk 501 (see Section 3.2), $t_{\text{var}} = 1$ d and $\delta = 10$, is at a distance $R = 0.4$ pc from the center. The thick solid curve shows the total spectrum of the escaping neutrons, and the dot-dashed curve shows the spectrum of gamma rays that could be produced by these neutrons outside the blob and escape the scattering region.

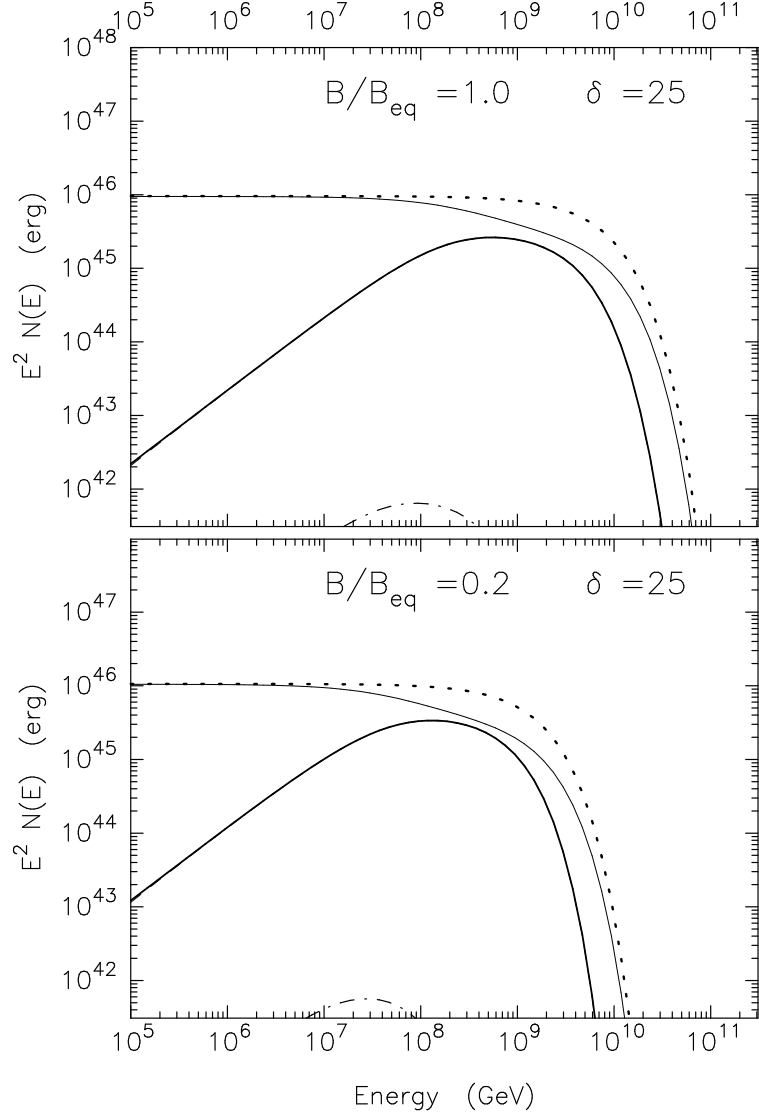


Fig. 7.— Energy spectra of protons neutrons, and gamma rays from a jet in Mrk 501 type object, as in Fig. 6, but calculated for the case $t_{var} = 0.1$ d and $\delta = 25$, with $B = B_{eq} = 1.0$ in (a), and $B = 0.2B_{eq}$ in (b).

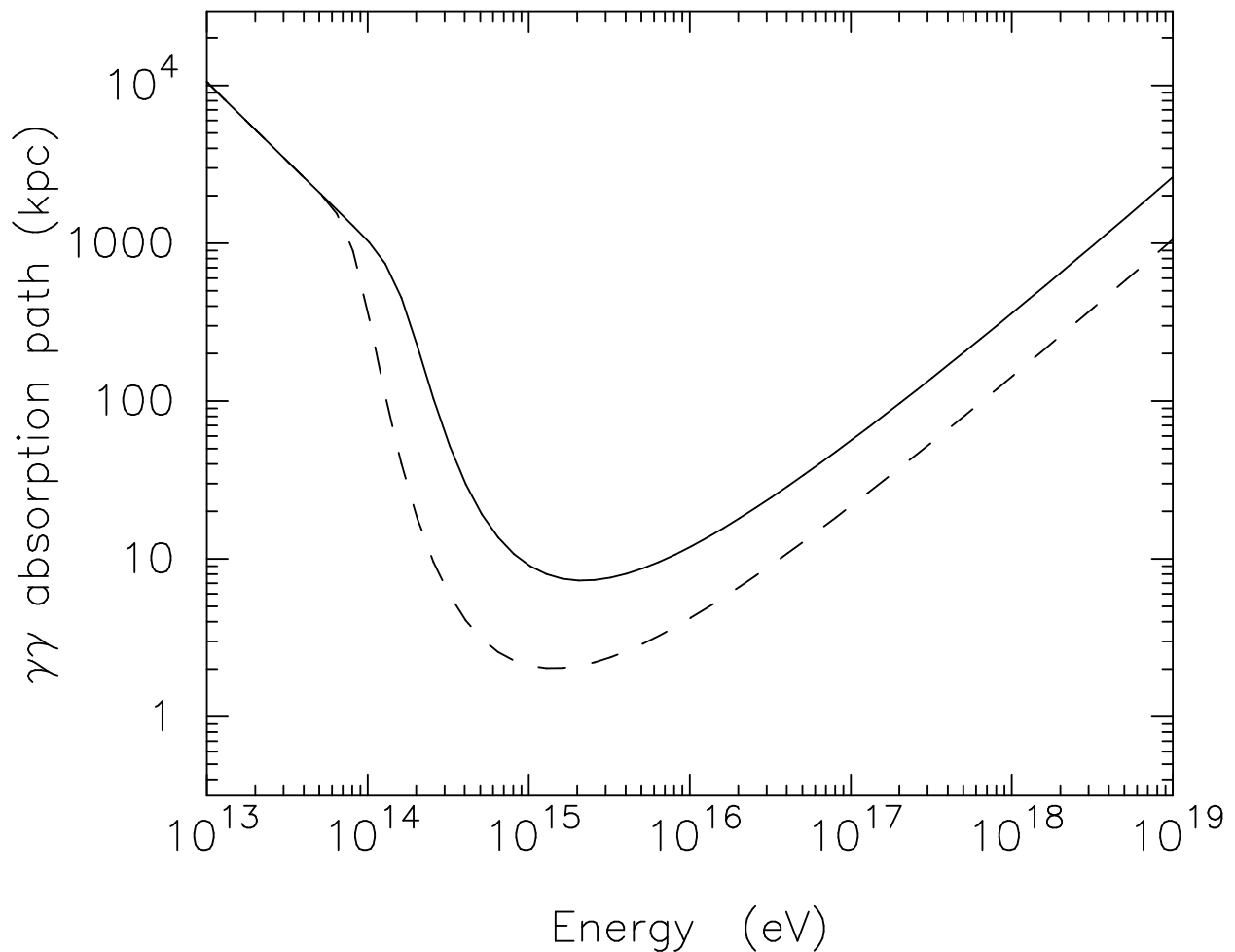


Fig. 8.— Mean-free-path of gamma rays due to pair production interactions with photons of the diffuse cosmic microwave background radiation for $z = 0$ (solid curve) and $z = 0.538$ (dashed curve), including the diffuse extragalactic infrared radiation field (see Section 4.3).